Title

Functional Dissection of a Viral DNA Packaging Machine's Walker B Motif

Journal

Journal of Molecular Biology, 431(22)

ISSN

0022-2836

Authors

delToro, Damian
Ortiz, David
Ordyan, Mariam
et al.

Publication Date

2019-11-01

DOI

10.1016/j.jmb.2019.08.012

Peer reviewed

HHS Public Access

Author manuscript

J Mol Biol. Author manuscript; available in PMC 2020 November 08.

Published in final edited form as:

J Mol Biol. 2019 November 08; 431(22): 4455–4474. doi:10.1016/j.jmb.2019.08.012.

Functional Dissection of a Viral DNA Packaging Machine's Walker B Motif

Damian delToro[1,†], **David Ortiz**[2,5,†], **Mariam Ordyan**[1,†], **Joshua Pajak**[3,†], **Jean Sippy**[4], **Alexis Catala**[1,6], **Choon-Seok Oh**[4], **Amber Vu**[4], **Gaurav Arya**[3], **Douglas E. Smith**[1,*], **Carlos E. Catalano**[2,7,*], **Michael Feiss**[4,*]

[1]Dept. of Physics, University of California, San Diego, La Jolla CA 92093

[2]Dept. of Medicinal Chemistry, University of Washington, Seattle, WA 98195

[3]Dept. of Mechanical Engineering and Materials Science, Duke University, Durham, NC 27708

[4]Dept. of Microbiology, Roy J. and Lucille A. Carver College of Medicine, University of Iowa, Iowa City, IA 52242

[5]Current Address, Department of Translational Sciences, Seattle Genetics, Inc., Bothell, WA 98021

[6]Current Address, Program in Structural Biology and Biochemistry, University of Colorado Denver, Anschutz Medical Campus, Aurora, CO 80045

[7]Current Address, Dept. of Pharmaceutical Sciences, Skaggs School of Pharmacy and Pharmaceutical Sciences, University of Colorado Denver, Anschutz Medical Campus, Aurora, CO 80045

Abstract

Many viruses employ ATP-powered motors for genome packaging. We combined genetic, biochemical, and single-molecule techniques to confirm the predicted Walker-B ATP-binding motif in the phage λ motor and to investigate the roles of the conserved residues. Most changes of the conserved hydrophobic residues resulted in $>10^7$-fold decrease in phage yield, but we identified nine mutants with partial activity. Several were cold-sensitive, suggesting that mobility of the residues is important. Single molecule measurements showed that the partially-active A175L exhibits a small reduction in motor velocity and increase in slipping, consistent with a slowed ATP binding transition, whereas G176S exhibits decreased slipping, consistent with an *accelerated* transition. All changes to the conserved D178, predicted to coordinate Mg^{2+}•ATP, were lethal except conservative change D178E. Biochemical interrogation of the inactive D178N protein found no folding or assembly defects and near-normal endonuclease activity, but a ~200-fold reduction in steady-state ATPase activity, a lag in the single-turnover ATPase time course, and no DNA packaging, consistent with a critical role in ATP-coupled DNA translocation. Molecular dynamics simulations of related enzymes suggest that the aspartate plays an important role in enhancing the catalytic activity of the motor by bridging the Walker motifs and precisely

*Correspondence to: michael-feiss@uiowa.edu, des@ucsd.edu, carlos.catalano@ucdenver.edu.
†These authors contributed to the work equally

contributing its charged group to help polarize the bound nucleotide. Supporting this prediction, single molecule measurements revealed that change D178E reduces motor velocity without increasing slipping, consistent with a slowed hydrolysis step. Our studies thus illuminate the mechanistic roles of Walker-B residues in ATP binding, hydrolysis, and DNA translocation by this powerful motor.

Keywords

terminase; molecular motor; virus assembly; nucleoprotein packaging complexes

INTRODUCTION

The assembly pathways of many large double-stranded DNA (**dsDNA**) viruses, including the herpesviruses and many tailed phages, include a DNA packaging step in which newly replicated viral genomes are packaged into preformed protein shells [1-5]. The packaging substrate is typically a multi-genome concatemer and the reaction is performed by a viral-encoded **terminase** enzyme. Terminases recognize viral DNA and cleave the polymeric packaging substrate at the beginning of one genome sequence. Following the initial DNA cleavage, terminase remains bound to the newly created genome end. The terminase-DNA complex next docks on the portal vertex of the icosahedral procapsid shell; the portal vertex is a dodecamer of radially disposed subunits with a central channel for DNA transit. Upon docking, terminase's packaging ATPase is activated to power translocation of the DNA into the procapsid. DNA packaging is terminated when terminase cleaves the DNA at the downstream end of the genome sequence and releases the DNA-filled capsid (Figure 1A) [6]. The ATP-fueled terminase motors are extremely powerful, generating very high forces (>50 pN) and translocating DNA rapidly (~600 bp/sec in phage λ) and with high processivity, ultimately packaging DNA to near crystalline density [2, 7-12]. While much is known about the structure function of these motors [13-27], the chemo-mechanics of translocation is not fully understood.

Terminases are generally hetero-oligomers of a small subunit (**TerS**) that specifically recognizes viral DNA and a large catalytic subunit (**TerL**) [1]. The TerL subunits possess C-terminal DNA processing endonuclease and N-terminal ATP hydrolysis-powered translocase activities required to mature and package the viral genome [1, 5, 20, 28-30]. Atomic structures of TerL subunits from phages T4, Sf6, P74-26, and D6E, and the packaging ATPase of phi29 [13, 19, 21, 31, 32] show that the N-terminal ATPase fold belongs to the oligomeric ring ATPases group of Additional Strand, Catalytic Glutamate (**ASCE**) ATPases [33-35]. This oligomeric ring ATPases include many cellular ATPases of diverse function that act in protein unfolding and degradation, protein transport and translocation, ATP synthesis, and DNA recombination reactions [35-38]. The ASCE fold is strongly conserved in both viral and cellular molecular motors and contains Walker A (**WA**) and Walker B (**WB**) motifs involved in ATP binding and hydrolysis. Extensive studies in a variety of

[1]For simplicity, we use TerL with a superscript designating the virus of origin; e.g., the large terminase subunit of T4 is designated $TerL^{T4}$ and that of λ is designated $TerL^{\lambda}$, etc.

cellular systems including the elongation factor EF-Tu, adenylate kinase and myosin [39-41] and in many phage genome packaging motors including T4, Sf6, P74-26, and phi29 [13, 19, 21, 31, 42] implicate specific roles for residues in these motifs, as follows. The classical WA signature sequence is [(G/A)XXXXGK(T/S)], where "X" represents a variable amino acid [43]. The conserved lysine ε-amino group coordinates the β- and γ- phosphates and the serine/threonine hydroxyl group coordinates the Mg^{2+} of the bound Mg^{2+}•ATP, positioning the β-and γ-phosphates for hydrolysis [19, 21, 31, 44, 45]. In addition, many viral packaging motors have been identified to have a conserved arginine at position 3 or 4 in the WA motif which has been implicated in ATP hydrolysis and chemomechanical coupling [13, 21, 25, 46]. Downstream from WA is the WB motif, whose classical signature sequence is ϕϕϕϕD, where ϕϕϕϕ indicates a quartet of hydrophobic residues; the conserved WB aspartic acid residue coordinates the Mg^{2+} of the bound Mg^{2+}•ATP, along with the WA serine/threonine [19, 21, 31, 44]. This conserved aspartate is distinct from a conserved "**catalytic glutamate**" that directly follows in the WB of ASCE ATPases (Figure 1B) and evidence suggests activates a water molecule for nucleophilic attack of the γ-phosphate [19, 21, 35, 44, 47-49] .

Before any TerL structures were known, pioneering work by Rao and co-workers predicted the locations of WA and WB ATPase motifs in a number of TerL proteins based on sequence alignments (Figure 1B) and confirmed the predictions for $TerL^{T4}$ via genetic and biochemical studies [29, 45-47, 50]. In genetic studies of the WA sequence, the Arg, Gln, Gly, and Lys residues could not be changed without loss of function, and for the Thr, only the conservative Ser substitution was functional [13, 29, 42]. Multiple residues in the $TerL^{T4}$ WB "hydrophobic quartet" could be changed without loss of function although the results supported the importance of hydrophobicity [45]. Any changes to the Asp were lethal and found to impair photo-affinity cross-linking by azido-ATP, indicating a nucleotide binding defect. In contrast, changes of the catalytic Glu did not abrogate azido-ATP binding, but did abolish ATP hydrolysis and DNA packaging [45, 47]. Subsequently, crystal structures of the phage T4, Sf6, P74-26, phi29, and D6E motor proteins confirmed the predicted WA and WB motifs [19, 21, 31, 32, 44].

The phage λ DNA packaging system is highly developed for genetic, biochemical and biophysical studies. Genetic studies implicate the N-terminal domain of TerL in DNA translocation [28], and azido-ATP cross-linking studies identified residues indicating the locations of the adenine binding and WA motifs [51]. Biochemical studies have elucidated the assembly of the terminase multimer, as follows. Terminase subunits form a stable $TerS_2$•$TerL_1$ protomer, which assembles at *cos*, the packaging initiation site in the λ concatemer, to afford a catalytically competent nuclease complex that "matures" the genome end in preparation for packaging [52]. The post-cleavage nucleoprotein complex then binds to the portal to afford the packaging motor complex that translocates DNA into the shell; biochemical studies indicate that the protomers are functionally coupled during DNA translocation [53].

Given the conservation of structural and functional features of ASCE domains, and specifically in the terminase enzymes, we embarked on an integrated genetic, biochemical and biophysical dissection of the ATPase domain $TerL^{\lambda}$ as a model system. We previously

applied this approach to characterize the functional roles of TerL$^{\lambda}$ residues in the adenine binding Q motif (N-linker), the coupling C motif (motif III) and a loop-helix-loop motif implicated in motor velocity [22, 23]. We further confirmed and characterized the proposed WA motif in TerL$^{\lambda}$ (^{76}-KSARVGYSK^{-84}) [25], in which the critical lysine is at the beginning of the WA motif (K76) rather than its typical position at the C-terminal end. The results from these studies led us to propose a model wherein ATP binding to TerL$^{\lambda}$ drives a conformational change that results in tight ATP binding *and* tight DNA gripping (Figure S1) analogous to the "tight binding transition" proposed previously for phage phi29 [17, 25] . More recently, we confirmed that TerL$^{\lambda}$'s catalytic glutamate is residue Glu^{179}. Changes eliminating the carboxylate functional group abolished ATP hydrolysis and DNA translocation [49]. Remarkably, we found that the conservative residue change E179D caused nearly identical perturbations of the translocation dynamics as change R79K to the conserved arginine in the WA motif. These findings suggested that both changes affect the chemo-mechanical ATP hydrolysis cycle in a similar way. Supporting this proposal, structure-based molecular dynamics simulations [49] predicted that the conserved catalytic glutamate, E179, and the conserved Walker A arginine, R79, interact and work in concert to bind ATP and align the hydrolysis transition state in an "open-to-closed" active site conformation that may be a common mechanistic feature in many terminases. In addition, the simulations and mutant findings provided evidence for an "arginine toggle" mechanism in which, after hydrolysis and product release, the WA arginine rotates away from the catalytic Glu to interact with a different Glu residue in the "lid" subdomain that is proposed to mediate chemo-mechanical coupling to drive DNA translocation. In summary, our integrated studies of TerL$^{\lambda}$ residues have confirmed many motif predictions and revealed that single amino acid changes affect not only ATP binding and hydrolysis, but also chemo-mechanical coupling, multi-subunit ring assembly and DNA translocation dynamics [22, 23, 25, 49].

In the present study, we extend our characterization of the ASCE domain and validate the assignment of the predicted ^{174}-VAGYD^{-178} WB motif in TerL$^{\lambda}$. More importantly, we define the role of these residues in motor function. Our findings indicate that the four hydrophobic residues, with a few exceptions, cannot be changed without loss of function, and suggest that they are important for both folding and domain mobility to facilitate interaction of the catalytic Glu with ATP. The data further confirm that D178 is critical for rapid DNA translocation, consistent with the predicted role in Mg^{2+}•ATP binding, and suggest that WB residues play an important role in properly positioning charge groups to catalyze hydrolysis. Given the conservation of structure and function of the ASCE ATPase domains, both viral and cellular, these insights into viral terminase function provide information that broadens our understanding of ATP-powered biomotors.

Results

Genetic Analysis: Functional Effects of Residue Changes.

Genetic Screen of the WB Hydrophobic Quartet.—Sequence analysis revealed that TerL$^{\lambda}$ residues ^{174}-VAGYD^{-178}, followed by the putative catalytic glutamate E179, are a good fit to the WB signature sequence (Figure 1B) and we first examined their roles using a

genetic screen. We surveyed the effects on phage yield of many single and double residue changes spanning the putative WB hydrophobic quartet (gene *A* codons 174 to 177). Mutagenesis was done using oligonucleotide primers with randomized bases in the target codons and, following sequencing, selected mutants were chosen for further study. A total of 32 residue changes were examined using a sensitive complementation assay [25] in which a plasmid was used to provide $TerL^{\lambda}$ (WT or mutant) to a defective phage at a level of expression approximating that during a normal virus infection. Specifically, the complementation plasmid supplies $TerL^{\lambda}$ to an inducible mutant prophage carrying two *A* amber mutations (λ *A*am), used to block normal TerL expression. When the plasmid provides functional $TerL^{\lambda}$ subunits to the induced λ *A*am prophage, packaging of the λ *A*am phage genome occurs and the yield of λ *A*am phage is determined by titering the lysate on a host containing the appropriate amber suppressor. This host allows the λ *A*am phage to produce WT terminase and form plaques, which are counted to determine the virus yield. Complementation with WT $TerL^{\lambda}$ typically produces a virus yield of 3-10 phages/induced lysogen; mutants expressing partially active $TerL^{\lambda}$ show intermediate yields of λ *A*am phages, reflecting the level of functional $TerL^{\lambda}$. In this manner, mutant terminases that sponsor small amounts of viral assembly, down to ~10^{-7} the level for the WT $TerL^{\lambda}$ plasmid, can be quantified. This approach provides much higher sensitivity to terminase activity than achieved by directly introducing $TerL^{\lambda}$ mutations into the viral genome and studying their effect on plaque formation, because for a λ strain to produce a plaque its yield must typically be greater than ~10% that of WT (green, Figure 2). From the complementation results, we thus refer to a mutation as “lethal” if the yield is lower than this amount even though much lower levels of viral assembly assay can be detected by the complementation assay.

As an initial test, we mutagenized the adjacent codon pairs ^{174}-VA^{-175}. In total, 19 double mutants were characterized. In stark contrast to findings in the phage T4 system which tolerated many residue changes, we found that only the TerL with the highly conservative VA→AV change supported a normal virus yield while 18 of the 19 double mutants were lethal (<10% yield) (Figure 2). Of the 18 lethal mutations only two, VA→GV and VA→GI, supported detectable levels of terminase function, with virus yield levels of 0.13 and 3.3 × 10^{-5} that of WT, respectively (Figure 2). The other 16 were profoundly defective (<10^{-7} that of WT), including the conservative VA→LL change. We similarly mutagenized the adjacent ^{176}-GY^{-177} codon pairs and all 9 of the double mutants were lethal changes, exhibiting various degrees of functional impairment; change GY→CW resulted in a lethal, 20-fold reduction while changes to EK, LC, or VF caused >10^{5}-fold reductions (Figure 2). The remaining tested residue changes were profoundly lethal, reducing the virus yield to a level below the sensitivity of the assay (i.e., by >10^{7}-fold). In addition to the double mutants above, a set of single mutants were tested to study the functional roles of individual hydrophobic quartet residues: Of these, A175L and G176S were viable, while V174P and Y177V were profoundly lethal (Figure 2).

Walker B Mutant Phages.—To confirm the results obtained from the complementation experiments above, we constructed lysogens carrying prophages with mutations expressing $TerL^{\lambda}$s with the viable VA→AV, A175L, G176S changes (Figure 2), as described in

Materials and Methods. Induction of the viable mutant prophages allowed us to characterize each mutant phage's ability to form plaques, which requires that a mutant phage produce a yield of at least about 15 virions/induced lysogen, i.e., ~10% of the wild type. The results confirmed the above complementation study: The viable mutants VA→AV, A175L, and G176S, produced robust, near-wild type yields at 37°C (Table S1).

We also tested the viable mutant phages for conditional lethality. The A175L phage forms small plaques at 42°C and 37°C, but none at 30°C, hence it is a cold-sensitive (cs), conditionally lethal mutant. The VA→AV phage formed small plaques at 42°C and 37°C, and tiny plaques at 30°C, indicating non-lethal cold sensitivity. The G176S phage, like the WT phage, forms large plaques at 42°C and 37°C and medium plaques at 30°C, indicating that this mutation has essentially WT phenotype.

Finally, we measured the virus yields for the non-plaque forming VA→GV and GY→CW mutant prophages. The parent phage into which WB mutations were placed carries a kanamycin resistance cassette (see Materials and Methods), which enables us to determine the yields of phages per cell for the lethal mutants, i.e., phages carrying the VA→GV and GY→CW changes, by measuring the number of kanamycin resistance transducing particles in a lysate. In agreement with the complementation results, we found that both mutant phage yields were somewhat below the threshold necessary for plaque, with the VA→GV and GY→CW phages having yields 2% and 4% that of the wild type phage, respectively (Table S1).

In sum, the complementation and phage yield assays indicate that all four of the hydrophobic residues spanning ^{174}-VAGY^{-177} in TerL$^{\lambda}$ are functionally important and, except for a few conservative changes, they cannot be changed without loss of function. The results support the proposal that these residues comprise the hydrophobic quartet of TerL$^{\lambda}$'s WB segment and, to a greater degree than for TerL^{T4}, show that this specific sequence is critical for efficient viral assembly. These TerL$^{\lambda}$ results indicate that additional properties of these residues besides just hydrophobicity are important. We note that these four residues are at the end of β strand 3 in the ATPase domain and the specific amino acid sequence is likely important, presumably for residue packing within the domain and/or proper positioning of the downstream ^{178}-DE^{-179} residues putatively involved in ATP binding and catalysis, respectively. That two of three viable mutants show cold sensitivity further suggests that mobility within the hydrophobic quartet, and thus β3, is important for terminase function; this is discussed further below.

The Conserved WB Aspartate.—We next examined the conserved TerL$^{\lambda}$-D178 residue, which has been implicated in coordinating the Mg^{2+} cofactor of the Mg^{2+}•ATP moiety in the ASCE enzymes. If D178 serves this role, then the expectation is that its carboxylate is critical for ATP binding and/or hydrolysis. The genetic results are in accord with these expectations; no changes to non-acidic residues (of 9 tested) produced terminase with detectable function (Figure 2). In addition to the complementation studies, a phage carrying the D178E codon, TerL$^{\lambda}$ -D178E, was constructed and found to form small plaques at 42°C, tiny plaques at 37°C and was unable to form plaques at 30°C, indicating that the D178E

change is a cold-sensitive conditional lethal mutant (Table S1). Thus, even this conservative TerL$^{\lambda}$-D178E change has significant functional effects.

Effects of WB mutations on gene expression and terminase assembly.—Based on studies in the T4 system, the lethal phenotypes of nearly all the TerL$^{\lambda}$ mutations examined was unexpected. A trivial explanation would be that the changes affect efficient expression of the protein as opposed to the desired effect of perturbing motor function (e.g., ATP binding, hydrolysis, chemo-mechanical coupling, etc.). To address this question, we examined WB mutant expression. Selected mutations, including ^{174}-VA^{-175}→GI, A175L, D178A, D178E, and D178N, were transferred to the terminase expression vector, pQH101alt. Following terminase expression, whole cell extracts were electrophoresed on SDS-PAGE gels and the Coomassie blue-stained gels showed that TerL$^{\lambda}$ is efficiently expressed by the WT and all the missense mutants examined (data not shown). Thus, these WB mutant enzymes do not have significant gene expression defects [25].

To test functional integrity, we next examined selected mutants, *in vitro*, to determine if they were folded and assembled properly, using the following approach. Because the introduced mutations reside in the N-terminal ATPase domain of TerL$^{\lambda}$, we expected them to selectively affect the ATPase (and thus DNA packaging) activity. The *cos*-cleavage endonuclease center resides in the C-terminal domain and should be unaffected if the mutant protein is folded and can assemble a functional maturation complex [28, 54] (Figure 1A). Thus, if holoterminase is properly folded and assembled, the mutant enzymes should retain normal *cos* cleavage activity in crude cell extracts. *In vitro cos* cleavage assays, done at 22°C, showed that of eight mutant enzymes examined, V174P, ^{174}-VA^{-175}→GI, Y177V (Figure 3), and D178A (not shown), lacked *cos* cleavage activity. Thus, these four mutants likely have defects in folding and/or assembly, which explains their lethal defect. However, the other four mutant enzymes, A175L, G176S, D178E (Figure 3), and D178N (*vide infra*), retained *cos* cleavage activity, which requires a folded and functional enzyme. These findings suggest that the WB residues play specific and significant roles in the folding and stability of an active terminase enzyme.

Finally, we were also curious about the cold-sensitivity of the D178E mutant phage (Table S1) and asked if this is the result of a stability defect of the mutant enzyme. To examine this possibility, we compared *cos*-cleavage activity of the D178E mutant enzyme at 22°C and 42°C (Figure 3B). No significant differences from wild type were found, indicating that the cold sensitivity of the D178E mutant does not involve the endonuclease activity at these temperatures.

Biochemical and Ensemble Biophysical Analysis of the TerL$^{\lambda}$-D178N Enzyme

Based on the genetic studies described above, we chose the TerL$^{\lambda}$-D178N mutant terminase for biochemical interrogation to probe for the mechanistic defect. This residue is proposed to coordinate Mg^{2+} to bind Mg^{2+}•ATP at the active site. Consistently, the mutation is lethal to phage growth (Figure 2) but retains WT *cos*-cleavage activity in the crude extract assay (not shown). This suggests that the enzyme is selectively defective in ATPase activity, and thus genome packaging, as predicted. To test this hypothesis, TerL$^{\lambda}$-D178N terminase was

expressed and purified as previously described [25, 53, 55]. The yield of mutant enzyme is similar to that of WT (not shown), suggesting that no significant structural defects resulted from the residue change. Consistently, the circular dichroism spectrum of the mutant protein is essentially identical to WT, indicating that the mutation does not affect the secondary structure of the protein (Figure 4A). We next examined the stability of the mutant enzyme, and Figure 4B shows that thermal denaturation of the TerL$^{\lambda}$-D178N enzyme mirrors that of the WT enzyme, an indication that tertiary structures have not been significantly affected. The terminase protomer is composed of one TerL subunit tightly associated with two TerS subunits and the protomers assemble into a functional ring-like complex [52, 55, 56]. Analytical ultracentrifugation analysis demonstrates that the mutant protein similarly associates into a stable protomer and that the protomer-ring equilibrium remains intact (Figure 4C). In sum, the data confirm that the TerL$^{\lambda}$-D178N mutant enzyme is appropriately folded in solution and retains WT quaternary interactions required to assemble a functional motor.

We next examined the catalytic activity of the enzyme. Consistent with the initial studies described above which used cell extracts, the *cos*-cleavage activity of purified TerL$^{\lambda}$-D178N is intact (Figure 5A); this indicates that the C-terminal endonuclease domain has not been affected by the mutation. In contrast, the steady state ATPase activity of the mutant enzyme is severely compromised (0.5% activity compared to WT). Consistent with this result, DNA packaging activity, which is fueled by ATP hydrolysis, is similarly compromised by the mutation (0.7% activity compared to WT, Figure 5A). To further probe the mechanistic basis for the ATPase defect, we examined single turnover ATP hydrolysis by TerL$^{\lambda}$-D178N terminase to probe the kinetics of the reaction. In this assay, enzyme is included in excess of the ATP substrate and catalysis is limited to a single event that includes ATP binding and hydrolysis steps; subsequent product release step(s) are not included in the kinetic time course. The data presented in Figure 5B demonstrate that while single turnover ATP hydrolysis is observed, it is severely compromised in the mutant enzyme compared to WT. The kinetic data were first analyzed according to a simple monophasic kinetic model, which describes the WT enzyme well (Figure 5B) and affords k_{obs} = (0.139 ± 0.016) sec^{-1} (Table 1). In contrast, the kinetic time course for the TerL$^{\lambda}$-D178N enzyme is poorly described by this simple model due to a distinct lag in product formation.

We previously demonstrated that the TerL$^{\lambda}$ WA R79A mutant had a similar kinetic lag and required a more complex kinetic model to explain the data [25]. Thus, we proposed a model that includes a slow, reversible step prior to the chemical step (e.g., ATP hydrolysis);

$$4^{*}\mathbf{P} + \mathbf{DNA} + \mathbf{ATP} \underset{k_{-1}}{\overset{k_1}{\rightleftharpoons}} \mathbf{P_4{\bullet}DNA{\bullet}ATP} \xrightarrow{k_2} \mathbf{P_4{\bullet}DNA{\bullet}ADP{\bullet}P_i} \quad (1)$$

where P represents the terminase protomer in solution, P_4•DNA•ATP represents the catalytically competent ATP-bound multimer assembled on DNA, k_1 and k_{-1} are the rate constants for the slow step prior to catalysis and k_2 is the rate constant for ATP hydrolysis (the chemical step). Importantly, this model simplifies to the monophasic one when k_1 is fast. As shown in Figure 5B, fitting of the ATP hydrolysis time course for TerL$^{\lambda}$-D178N to the three-state model significantly improves the quality of the fit. The observed rate constant

for ATP hydrolysis by TerL$^{\lambda}$-D178N is 1.7% that of the WT enzyme (k_2 vs. k_{obs}, Table 1), consistent with the steady-state ATPase data (Figure 5A). Importantly, the slow step prior to hydrolysis (k_1) is significantly slower than would be anticipated from a diffusion-controlled ATP binding encounter (10^8-10^9 $M^{-1}s^{-1}$), consistent with a slow conformational change prior to catalysis [25].

Single Molecule Measurements of DNA Translocation Dynamics

Selected mutants were chosen for further analysis by a single-molecule assay we developed that directly measures DNA translocation dynamics [9, 22, 23, 25, 49, 57]. Partly pre-packaged procapsid-motor-DNA complexes are attached to a microsphere trapped with optical tweezers and the external end of the DNA molecule being packaged is attached to a second trapped microsphere. As the DNA is packaged the two microspheres are pulled together and increasing DNA tension is measured. The separation between the two traps is controlled by a feedback system which maintains a small tension of 5 pN to keep the DNA stretched while it is translocated, allowing the length of DNA packaged vs. time to be measured (Figure 6) [9, 57]. The measurements were made with saturating ATP (0.5 mM), low capsid filling (0-20% of the genome length packaged), and at room temperature (~23 °C). From these measurements we derive the overall packaging rate, the “motor velocity” (translocation rate not including pauses and slips), the frequency of slipping and pausing, and duration of pauses. As discussed below and in prior work [25, 49], relative changes in motor velocity and slipping shed light on residues involved in the ATP binding step versus those involved in the chemical hydrolysis step, while changes in pausing shed light on residues involved in proper alignment of ATP in the binding pocket.

The Hydrophobic Quartet.—To investigate roles of the four predicted hydrophobic WB residues we examined four examples of single residue changes, one at each position: V174P, A175L, G176S, and Y177V. We also studied one double residue change mutant (^{174}VA^{175}→GI), of interest because it exhibited a detectible, though highly reduced phage yield in the genetic studies (Figure 2).

Genetic studies found no detectible phage yield in the complementation assay for mutants V174P and Y177V and consistently, no DNA translocation activity was detected for either of these mutants despite hundreds of trials (Figure 7). As described above, this lack of activity is likely due to perturbation of the predicted hydrophobic β-sheet by these changes and defects in enzyme folding or assembly (Figure 3). The ^{174}-VA^{-175}→GI double mutant exhibited a small phage yield despite folding defects (*vide supra*) and Figure 7 shows there was no detectible DNA translocation activity despite hundreds of trials. Together, these findings suggest that while the efficiency of packaging initiation by ^{174}-VA^{-175}→GI is very low *in vitro* (<1%), at least some motors can package the full-length genome *in vivo* and afford infectious phages.

In contrast to the above findings, change A175L, which increases hydrophobicity and side chain bulk, resulted in only minor impairments in translocation activity (Figure 7); this is consistent with the finding of a phage yield similar to WT in the genetic studies (Figure 2). More specifically, the average motor velocity nominally decreased by ~10%, slipping

frequency increased ~2-fold, pausing frequency increased ~30%, and the duration of pauses increased ~2.4-fold (Figures 6 and 7). An increase in slipping with decreasing motor velocity is consistent with the trend measured for WT with decreasing [ATP] (Figures 7 and 8), which suggests that the residue change slightly slows the ATP tight binding transition (see Supplemental Figure S1) [25]. The increased pause duration further suggests that the residue change results in intermittent binding of ATP in a misaligned orientation that delays ATP hydrolysis and coupled DNA translocation.

The near wild-type translocation activity of the TerL$^{\lambda}$-A175L enzyme at room temperature (23°C) appears to contrast with the cold-sensitive phenotype of the phage carrying the A175L change (Table S1). However, this likely reflects differences in what is measured in the two techniques. The single molecule study measures the initial stages of packaging (<20% of the genome length packaged) while virus yield requires packaging of the complete genome. Together these findings suggest that viral assembly is impaired because of failure to efficiently package the entire genome due to a failure of the motor to overcome the large internal forces resisting DNA confinement that build up during the latter stages of packaging the full-length genome. To investigate this further, we conducted translocation measurements with 5x higher applied force (25 pN), which mimics the load forces on the motor caused by forces resisting DNA confinement encountered in the latter stages of packaging [14, 26]. Under these conditions, we found that the average motor velocity for the WT enzyme is 41% that measured at low force, while for the mutant motor it is 32% that observed at low force. Thus, the mutant motor is more sensitive to load force and this could explain its failure to sponsor efficient viral assembly because this difference could be further magnified as packaging progresses towards the end of the genome.

Finally, we examined the TerL$^{\lambda}$-G176S enzyme. This residue change, which did not significantly alter phage yield, also did not impair translocation activity. The average motor velocity and packaging rate are consistent with the WT values (Figure 7). A particularly striking finding is that the mutant motor exhibited 5-fold *less* frequent slipping (i.e., 5-fold higher processivity) than the WT motor, which suggests that the residue change results in an *accelerated* ATP tight binding transition (see Supplemental Figure S1) [25]. This is discussed further below.

The Conserved WB Aspartate.—We next analyzed the effects of changes in residue TerL$^{\lambda}$-D178, predicted to coordinate the Mg^{2+} of the bound Mg^{2+}•ATP. Changing the negatively-charged Asp to Ala or to Asn (an uncharged side chain of similar size) resulted in no measured translocation despite several hundred trials (Figure 7). These results are consistent with both the genetic study, which detected no virus yield with either of these mutant phages (Figure 2) and the biochemical studies, which demonstrated that ATP hydrolysis and DNA packaging by TerL$^{\lambda}$-D178N protein is severely compromised (Figure 5).

Only the TerL$^{\lambda}$-D178E mutant, having a conservative residue change that preserves negative charge, exhibited measurable translocation activity in the single-molecule assay. Even though this residue change lengthens the amino acid side chain by only one carbon bond length, the impairment in translocation dynamics is notably more severe that that observed

in response to the A175L change discussed above. Specifically, the D178E change resulted in a ~2.5-fold reduction in motor velocity (Figures 6 and 7). However, the slipping frequency did not increase (Figure 8), suggesting that it is the ATP *hydrolysis* chemical step that is slowed, not the ATP *tight binding* transition [25, 49]. In addition, a ~3-fold increase in pausing frequency and ~2-fold increase in pause duration was observed, suggesting that the residue change also results in intermittent binding of ATP in a misaligned orientation in which hydrolysis does not occur. This finding of significantly impaired translocation dynamics at room temperature is consistent with the finding that the D178E change is lethal at 30°C.

In summary, the combined genetic, ensemble biochemical, and single molecule data support the conclusion that residue D178 plays a critical role in coupled ATPase and DNA translocation functions.

Molecular Dynamics Simulations—To gain further mechanistic insight into the observed defects introduced by TerL$^{\lambda}$-D178 WB mutations discussed above, we employed molecular dynamics (**MD**) simulations. Since there is no solved structure of TerL$^{\lambda}$, we used the available TerL crystal structures of phages T4 (**TerL^{T4}**), P74-26 (**TerL$^{P74\text{-}26}$**), and Sf6 (**TerL^{Sf6}**) as model systems; these three proteins are closely related to TerL$^{\lambda}$ within the terminase subfamily of ASCE ATPases. Importantly, TerL^{T4} and TerL^{P74-26} share the conserved WB C-terminal aspartate studied experimentally in TerL$^{\lambda}$, whereas TerL^{Sf6} possesses a deviant penultimate glutamate (E118) (labelled in red in Figure 1B). We reasoned that modeling TerL^{T4} and TerL^{P74-26} and contrasting with TerL^{Sf6} could provide valuable insight into conserved WB mechanisms across the terminase enzyme family, which would complement our experimental data obtained with TerL$^{\lambda}$. To this end, we performed all-atom, explicit solvent MD simulations of TerL^{T4}-D255(N/E) and TerL^{P74-26}-D149(N/E) mutant enzymes and compared them with corresponding WT simulations. Our goal was to elucidate the mutation-induced rearrangements within the ATP-binding pocket that are responsible for aberrant ATP hydrolysis and coupled DNA translocation.

Wild Type TerL Simulations and the ATP-Tight-Binding Transition.—Simulations of all three TerLs reveal that the conserved WB D (E in the case of TerL^{Sf6}) fulfills its predicted role of chelating Mg^{2+} through a water molecule (Figure 9A-C). In addition, the simulations highlight the importance of a conserved stabilizing hydrogen bond between the WB D/E carboxylate groups and the conserved WA C-terminal (T/S) hydroxyl group, which has also been implicated in Mg^{2+} coordination [19, 21]. This predicted interaction is apparent in the nucleotide-bound crystal structure of TerL^{P74-26} and is even maintained by the deviant TerL^{Sf6}-E118 residue, despite its 1.5 Å-longer side chain. To compensate for the longer side chain, the backbone of TerL^{Sf6}-E118 is farther away from the conserved WA (T/S) (Table 2) such that the WB E carboxyl group is placed in a nearly identical functional position relative to the WA (T/S) hydroxyl group. We note that while the WA-WB interaction is not observed in the TerL^{T4} crystal structure, the published structure is that of a WB D255E/E256D double mutant which directly affects this interaction; however, our simulations predict that this interaction is indeed present in the wild-type TerL^{T4}.

The active site geometry described above leads to "multibody" interactions, whereby the WB (D/E) not only positions the WA (T/S) such that its oxygen points towards Mg^{2+}, but could also polarize its hydroxyl group to increase the strength of the coordination interaction with the Mg^{2+} ion. Moreover, we find that the WB Asp and WA (T/S) interaction is promoted by ATP binding. Specifically, apo state simulations of $TerL^{T4}$ and $TerL^{P74-26}$ predict a 9.5 and 8.6 Å backbone distance between the WB Asp and the WA (T/S) respectively, which shortens to 7.1 and 6.5 Å upon ATP binding (Table 2). Thus, the Walker motifs close around the Mg^{2+}•ATP complex as part of the tight-binding transition (Figure S1). In contrast, the backbone distance does not change much from apo to ATP-bound state in the $TerL^{Sf6}$ system because the hydrogen bond between WB E118 and WA S29 is maintained in the apo state in both crystal structure and MD simulations [19].

Null WB Asp Mutant Simulations.—We next performed simulations of $TerL^{T4}$-D255N and $TerL^{P74-26}$-D149N mutant enzymes generated *in silico* to model the null $TerL^{\lambda}$-D178N mutation studied experimentally. Unlike the WT proteins, these variants do not support the formation of a hydrogen bonding network which directly connects the WA and WB motifs discussed above. Rather, the δ-positive NH_2 group promotes interactions with exposed backbone oxygen atoms which repositions the mutant WB Asn sidechain to the WB side of the binding pocket (Figure 9D-E); this increases the distance between the WA and WB motifs (Table 2). Notably, the Asp→Asn mutation also hinders the movement of the conserved WA Arg (the "arginine toggle") into the binding pocket, which has been previously shown to be a crucial step in the tight-binding transition [49] (Figure S2 A-D). Accordingly, the lid subdomain of the ATP-bound Asp→Asn mutants is positioned like apo WT enzymes and not rotated as observed in the ATP-bound WT enzymes (Figure S3). This agrees with the experimental assignment that the Asp→Asn mutation not only affects ATP hydrolysis, but also impairs the tight-binding transition.

Functional WB Asp Mutant Simulations.—Finally, we performed simulations of $TerL^{T4}$-D255E and $TerL^{P74-26}$-D149E mutant enzymes to model the analogous $TerL^{\lambda}$-D178E mutation studied experimentally. Simulations of both mutant systems predict defects which can account for a slowed rate of hydrolysis, via *two* distinct mechanisms. First, our simulations predict that the longer side chain in $TerL^{T4}$-D255E forms a new interaction with the critical WA lysine K166 (Figure 9F, Figure S4). This causes the WA motif to improperly position the γ-phosphate of ATP, which in turn increases the distance between the γ-phosphate and the catalytic glutamate residue (Figure S5). Notably, a similar interaction between D255E and K166, along with the subsequent mis-coordination of γ-phosphate, are also observed in the crystal structure of the $TerL^{T4}$-D255E/E256D double mutant enzyme (Figure S6). In contrast, $TerL^{P74-26}$-D149E simulations do not predict that the mutant D149E would interact with the critical WA K43. Instead, the mutation is found to disrupt the ability of the WB residue to properly chelate Mg^{2+} through a water molecule. The mutant side chain directly chelates the Mg^{2+} ion, which displaces WA S44 and prevents it from coordinating with the Mg^{2+} ion (Figure 9G). Although this direct interaction does not significantly increase the distance between the catalytic glutamate and the γ-phosphate as observed in $TerL^{T4}$-D255E simulations, the positive electrostatic potential within the binding pocket is reduced (Figure 10). This result implies the electron density on the γ-

phosphate may not be as strongly polarized towards its surrounding oxygen atoms as in WT, which would destabilize the transition state and slow hydrolysis. Importantly, the WT-like interaction between the catalytic glutamate and the arginine toggle is conserved in both TerL^{T4}-D255E and TerL^{P74-26}-D149E (Figure S2E-F), suggesting that this mutation does not impair the tight-binding transition as dramatically as its D149N counterpart. Thus, our results discussed above suggest two distinct mechanisms by which the WB Asp→Glu change could impair the hydrolysis chemical step.

Discussion

The data presented above clearly demonstrate that residues ^{174}-VAGYD-^{178} in TerL$^{\lambda}$ are essential to motor function and phage development, and strongly support the WB motif assignment. More importantly, the results provide mechanistic insight into the role each residue plays in protein folding, motor assembly, and catalytic activities required to package the viral genome.

The TerL$^{\lambda}$ Hydrophobic Quartet.

WB residues ^{174}-VAGY^{-177} are theorized to function in the folding and stability of the core β-sheet of the ATPase domain [45]. Thus, it is not surprising that most mutations strongly affect virus development, presumably due to protein folding defects and/or perturbations in the positioning of critical ATP binding (D178) and catalytic (E179) residues. Consistent with this hypothesis, almost all changes in the hydrophobic residues are profoundly defective in sponsoring λ phage assembly and many are devoid of *in vivo* endonuclease activity, an indication that the mutant proteins fail to fold properly. Interestingly, the observed degree of lethal phenotypes in TerL$^{\lambda}$ contrasts sharply with results observed in the phage T4 system where many WB hydrophobic mutants showed no evidence of assembly defects and many conservative changes are tolerated [45]. Similar differences in tolerance to residue changes were observed in studies of phage T4's WA motif [25]. It is unclear why TerL^{T4} is more plastic than TerL$^{\lambda}$, but speculative possibilities are: (1) many substitutions in TerL$^{\lambda}$ affect protein folding and/or stability while TerL^{T4} is more robust structurally; [2] (2) The λ motor is only known to function as a heterooligomer of TerL plus TerS subunits both *in vitro* and *in vivo*, whereas *in vitro* it has been found that the T4 motor can function as a pentamer of TerL only. Thus, there may be an additional layer of structural complexity in the λ motor that requires functional interactions with TerS and DNA and that may be more sensitive to mutation; (3) The expression of TerL$^{\lambda}$ is limited [58] and may be significantly lower than that of TerL^{T4} *in vivo*. This may reflect important life style differences between the two phages. TerL^{T4} endonuclease activity is toxic to *E. coli* [54, 59]. For a virulent phage such as T4, every infection kills the host cell, so production of a high level of TerL^{T4} is inconsequential. In contrast, temperate phages such as λ must allow lysogenization, which requires that a toxic level of TerL$^{\lambda}$ expression be avoided [59, 60]. Consequently, TerL$^{\lambda}$ expression during a productive λ infection is very low and a mutant enzyme with a partial defect in folding or assembly is expected to have a more detrimental effect on phage yield.

[2]We note, however, that the lethal TerL$^{\lambda}$-D178N change does not cause a major folding defect and any mis-folding would be highly localized within the ATP binding pocket of the enzyme.

Among the viable WB mutants in TerL$^{\lambda}$, we note that A175L is cold-sensitive and the ^{174}-VA^{-175}→AV is cold compromised, i.e., makes tiny plaques at the cold temperature. This mirrors observations with TerL^{T4} in which several WB mutants were found to be cold-sensitive [45]. One interpretation is that the activity of ATPase center has specific sequence requirements, beyond simple hydrophobicity, that are perturbed by mutation of residues within the quartet. Specifically, these residues may serve to properly position the Mg^{2+}-coordinating D178 residue and the adjacent catalytic E179, and perhaps allow dynamic mobility to these residues to efficiently catalyze hydrolysis. Within this context, it is interesting that a variety of motor translocation phenotypes were observed in enzymes with altered hydrophobic residues in the optical tweezer studies, as discussed next.

In contrast to the lethal mutations in the hydrophobic quartet discussed above, the Ter$^{\lambda}$-A175L mutant, which increases residue hydrophobicity and side chain bulk, is viable and exhibits only minor impairments in DNA translocation. Our findings support that A175 plays a role in ATP binding, presumably by helping to position the nearby D178 residue that coordinates the Mg^{2+} of Mg^{2+}•ATP. The near-WT level of activity of the A175L mutant suggests that A175 does not play as significant a role in protein folding as the other three hydrophobic WB residues.

The Conserved WB Aspartate.

TerL$^{\lambda}$-D178 is the predicted conserved WB residue that chelates Mg^{2+}•ATP to appropriately position the bound γ-phosphate for hydrolysis [45]. Our genetic studies found that all tested changes of TerL$^{\lambda}$-D178 are lethal, with the most conservatively changed mutant, D178E, being a conditional (cold-sensitive) lethal mutant. In addition to structural defects associated with this mutant, single molecule studies reveal defects in DNA translocation dynamics and shed further light on the nature of the defect. First, the significant decrease in motor velocity without significant increase in slipping suggests that the defect is not due to a slowed ATP tight binding transition, but is caused by perturbation of the activity of the adjacent catalytic carboxylate (E179) and a concomitant decrease in ATP hydrolysis [25, 49]. Within our kinetic model (Figure S1), slowing the chemical step (ATP hydrolysis) slows the motor without causing increased slipping [25], as is observed.

Second, change D178E causes a ~3-fold increase in the average frequency of motor pauses and ~2-fold increase in average duration of pauses (Figure 7). Intermittent pausing of the WT motor increases with decreasing [ATP], which we previously attributed to an off-pathway state in which terminase intermittently grips DNA tightly despite not undergoing the ATP tight binding change [25]. However, since D178E's infrequent slipping is inconsistent with a slowed ATP tight binding conformational change (*vide supra*), its increased pausing must be attributed to a different effect. A similar phenotype was observed previously in response to change R79K in the WA motif. Our interpretation is that both mutations result in intermittent binding of ATP in a misaligned orientation that allows tight DNA gripping but does not permit catalysis of hydrolysis, as proposed previously [25]. This finding implicates residue TerL$^{\lambda}$-D178 as playing an important role in proper ATP alignment, which has also been suggested previously for the analogous residue in TerL^{T4} [45]. The temperature sensitive behavior of the D178E enzyme in the genetic studies, in

which plaques were only obtained at 37°C and 42°C, may be related to these effects. Increased plasticity of the active site with increasing temperature may allow proper alignment of the bound Mg^{2+}•ATP into a catalytically competent conformation and a functional packaging motor to accommodate the $TerL^{\lambda}$-D178E change.

Despite the cold-sensitive phenotype, $TerL^{\lambda}$-D178E mutant terminase sponsors viable phage production at elevated temperatures. Thus, mutant WB glutamate (E) in $TerL^{\lambda}$ functions as well as the WT aspartate (D), likely because both are acidic residues that have similar size and negative charge. Within this context, sequence alignments predict that some terminases such as those of phages SPP1 and Sf6, classified as “Deviant I” types, utilize a Glu at this position rather than an Asp [45]. Our finding that the $TerL^{\lambda}$-D178E mutant can sponsor translocation, albeit impaired at room temperature, supports the notion that the Glu residues in those systems could function analogously to $TerL^{\lambda}$-D178.

The biochemical characterization of the $TerL^{\lambda}$-D178N mutant enzyme is also informative. This mutation does not affect folding or stability of the protein nor the maturation activity of the enzyme. The D→N change selectively affects ATP hydrolysis and thus packaging. Interestingly, there is a kinetic lag in the single-turnover time course which can be attributed to a rate limiting step prior to the chemical step that is not observed in the WT enzyme. Prior studies demonstrated a similar ATPase kinetic lag in the WA $TerL^{\lambda}$-R79A mutant enzyme that also exhibited a kinetic lag in *cos*-cleavage activity. In that case, the mutation caused a slow rate of motor assembly on viral DNA [25]. In contrast, while there is a distinct kinetic lag in single turnover ATP hydrolysis by the D178N mutant enzyme, there is no indication of a lag in the *cos*-cleavage time course (not shown). Thus, the nature of the lag in ATP hydrolysis must be distinct from that observed with the WA mutant enzyme characterized previously and we suggest that it is the result of slowed ATP-binding. Since the rate constant obtained in the kinetic fit is significantly less than that expected for diffusion-controlled ATP binding (~10^7– 10^8 M^{-1}•sec^{-1}; [61]), it is likely that this represents the ATP tight binding transition discussed above, and the kinetic data provide a rate of (1.7 ± 0.2) x 10^4 $M^{-1}sec^{-1}$ for this conformational change (Table 1).

Insights from simulations.

Our MD simulations identify a stable hydrogen bond between the conserved WB (D/E) and WA (T/S) residues in TerL proteins that is promoted by Mg^{2+}•ATP binding. In fact, simulations suggest that the backbones of the TerL proteins may be tuned to the size of the WB (D/E) side chain such that this interaction is conserved upon ATP binding. That is, $TerL^{Sf6}$ positions its “deviant” WB Glu ~1.4 Å farther away from the WA Ser than $TerL^{P74-26}$ positions its WB Asp to accommodate a 1.5 Å longer side chain. Structural and mutagenesis studies suggest that a similar hydrogen bond between the conserved WB Asp residue and the conserved WA Ser is crucial for function in the MRP1-NBD1 multi-drug resistance ATPase [62].

Our MD studies on the two null mutant model systems, $TerL^{T4}$-D255N and $TerL^{P74-26}$-D149N, intended to be analogous to the $TerL^{\lambda}$-D178N mutant studied experimentally, further suggest that this hydrogen bond is critical for motor function. The mutant residue no longer interacts with the WA (T/S) across the binding pocket, but instead remains isolated on

the WB side due to new interactions between the mutant NH_2 group and exposed backbone oxygen atoms. Loss of motor function is, in part, attributed to the loss of this hydrogen bond.

Our MD studies on the two functional mutant model systems, $TerL^{T4}$-D255E and $TerL^{P74-26}$-D149E intended be analogous to the $TerL^{\lambda}$-D178E mutant studied experimentally, predict distinct mechanisms for the disruptive effects on packaging. However, we propose that the effect of the $TerL^{\lambda}$-D178E mutation is more likely to be like that predicted for $TerL^{P74-26}$ D149E, in which the longer side chain directly chelates Mg^{2+} and perturbs its interaction with the conserved WA serine residue. In contrast, simulation of $TerL^{T4}$-D255E predicts that a new interaction is formed with the critical WA K166, consistent with mutant structural data.

We propose that the distinction in motor function between the two $TerL^{\lambda}$ variants (Asp→Asn and Asp→Glu) rests primarily in the tight-binding transition; while kinetic analysis implied that the Asp→Asn mutation impairs the tight-binding transition, the Asp→Glu mutation does not. One possible explanation is revealed by the MD simulations. While the Asp→Glu mutation does indeed affect binding pocket coordination, the mutant Glu exhibits defective coordination: it is predicted to directly chelate Mg^{2+} in $TerL^{P74-26}$ D149E or to hydrogen bond to the critical WA Lys in $TerL^{T4}$ D255E. In contrast, the Asp→Asn mutant does not directly participate in these types of interactions.

Engineering Improved Motor.

Unlike all other TerL mutants examined to date, the $TerL^{\lambda}$-G176S enzyme sponsored translocation at a rate equal to or slightly higher than the WT rate and remarkably exhibited 5x *higher* processivity (Figure 8). This behavior may be contrasted with those of previously studied WA mutants $TerL^{\lambda}$-Y82A and $TerL^{\lambda}$-S83T; both enzymes similarly exhibited increased processivity but significant *decreases* in motor velocity. The $TerL^{\lambda}$-G176S change thus causes an overall enhancement in function - increased processivity with no concomitant decrease in motor velocity. On the surface, this suggests that the motor can be engineered to have improved function through a single residue change. However, since slipping of the WT motor is quite infrequent, the improved processivity exhibited by $TerL^{\lambda}$-G176S does not result in a significant increase in the overall packaging rate (Figure 7). This suggests there would not be much natural selection pressure for the motor to evolve in this manner. Moreover, the higher slipping exhibited by the WT motor could even be advantageous to slow packaging to help mitigate the formation of unfavorable or “jammed” non-equilibrium states of DNA packaged into the procapsid [63-65]. In any case, we note that the ability to artificially engineer the motor to have improved processivity (reduced slipping) could be useful for applications in biotechnology, such as in the use of DNA translocating motors in nanopore-based single DNA molecule sequencing [66].

Conclusions

We have examined the role of WB motif residues in viral packaging motor function using a combination of genetic, biochemical, biophysical, and computational techniques. Our studies validate the proposed WB motif assignment in phage λ terminase and identify several mutants with partly-impaired DNA translocation and viral assembly activities that

shed light on the role of WB residues in motor function. Only a few residue changes are tolerated, and single molecule measurements show that WB residues play a role in determining motor velocity, processivity, and pausing. Our experimental results, and molecular dynamics simulations of related TerL enzymes, support the prediction that the conserved WB aspartates play an important role in ATP binding and further suggest that the hydrophobic WB residues play a role in positioning the catalytic glutamate to facilitate catalysis of ATP hydrolysis.

Materials and Methods

Microbiological techniques

Mutations affecting WB codons were introduced using splicing-by-overlap-extension and mutagenic PCR techniques to generate the desired codon changes [67]. Care was taken to avoid mutant codons rarely used in *E. coli*. Mutations were introduced into the complementation plasmid, pJM5alt, and the expression plasmid, pQH101alt, using standard molecular genetic manipulations. Complementation plasmid pJM5alt contains the λ DNA segment extending from the late gene promotor through *cos* and the terminase genes. Expression plasmid pQH101alt contains the terminase genes downstream of the strong early gene promotors P_R and P_L [68]. Transfer of mutations into both plasmids was facilitated by introduced restriction enzyme sites created by silent mutations in the *A* gene [25].

The method for introducing terminase mutations into phage λ [69] is described here briefly. The phage into which mutations were crossed was λ-P1:5R Kn^R *cI857 nin5 cos2*, hereafter called λ *cos2*. The *cos2* mutation is a lethal deletion of *cosN*, the cohesive end site, so λ *cos2* was maintained as a prophage. λ *cos2* produces the heat-labile *cI857* repressor and enters the lytic cycle when a culture growing at 30°C is shifted to 42°C to inactivate the repressor. After heat induction for 15 min, the culture is aerated at 37°C until cell lysis. The *cos2* mutation prevents DNA packaging, so no infectious virions are produced. To cross an *A* gene mutation into phage, a mutation-containing derivative of pJM5alt is introduced into *E. coli* (λ *cos2)*. The segment of λ DNA in pJM5alt includes $cosN^+$. If induced λ *cos2* rescues $cosN^+$ from the plasmid, the resulting phage DNA can be packaged to form infectious virions. The segment of plasmid DNA recombined into λ *cos2* frequently contains the plasmid *A* gene, including an *A* mutation. The lysate from such a cross is used to infect *E. coli* and resulting lysogens are selected by plating for kanamycin-resistant (Kn^R) transductants. Kn^R transductants are screened for inability to produce viable phages and/or sequencing the appropriate segment of the *A* gene.

Virus yield measurements were carried out as describe previously [25]. Note that in the complementation assay, the yield of the test phage (λ *cI857 red3 Aam11 Aam32*) was in the range from 6-to-10 phages/induced cell. The low yield is as expected for a red^- phage in a $recA^-$ host [70].

Biochemical Methods.

Terminase expression, purification and structural characterization was performed by published procedures [25, 53]. The *cos*-cleavage, DNA packaging and ATPase assays were performed as previously described [25, 71, 72].

Single-Molecule Methods

The optical tweezers instrument was calibrated as described previously [73, 74] and samples were prepared and single-molecule measurements were conducted as described previously [25, 57, 75].

Simulation Methods

100 ns long, all-atom, explicit solvent simulations were performed in triplicate using Amber16. Systems were at 150 mM salt concentration, 310 K, and 1 bar as described previously [49]. WB Asp→Asn and Asp→Glu mutations were introduced to the $TerL^{T4}$ and $TerLP^{74\text{-}26}$ systems in the same manner as the catalytic Glu→Asp mutations described previously [49]. Electrostatic potential surfaces were calculated with the APBS extension implemented in UCSF Chimera [76].

Supplementary Material

Refer to Web version on PubMed Central for supplementary material.

Acknowledgements

We thank Dr. David Baker (University of Washington) for access to the CD spectrometer. This work was supported by NIH awards R01-GM088186 and R01-GM118817. A.V. was supported by NSF-REU program in the Department of Microbiology at The University of Iowa under Grant No. DBI-7290775. Computational resources were provided by the NSF XSEDE Program under grant ACI-1053575 and the Duke Computer Cluster.

REFERENCES

[1]. Rao VB, Feiss M. Mechanisms of DNA packaging by large double-stranded DNA viruses. Annual review of virology. 2015;2:351–78.

[2]. Chemla YR, Smith DE. Single-molecule studies of viral DNA packaging In: Rao V, Rossmann MG, editors. Viral Molecular Machines. Boston, MA: Springer; 2012 p. 549–84.

[3]. Catalano CE. Viral Genome Packaging Machines: Genetics, Structure, and Mechanism. New York, NY: Kluwer Academic/Plenum Press; 2005.

[4]. Hetherington CL, Moffitt JR, Jardine PJ, Bustamante C. Comprehensive Biophysics Comprehensive Biophysics: Academic Press; 2012 p. 420–46.

[5]. Casjens SR. The DNA-packaging nanomotor of tailed bacteriophages. Nature Reviews Microbiology. 2011;9:647–57. [PubMed: 21836625]

[6]. Earnshaw WC, Casjens SR. DNA packaging by the double-stranded DNA bacteriophages. Cell. 1980;21:319–31. [PubMed: 6447542]

[7]. Smith DE, Tans SJ, Smith SB, Grimes S, Anderson DL, Bustamante C. The bacteriophage phi29 portal motor can package DNA against a large internal force. Nature. 2001;413:748–52. [PubMed: 11607035]

[8]. Fuller DN, Raymer DM, Kottadiel VI, Rao VB, Smith DE. Single phage T4 DNA packaging motors exhibit large force generation, high velocity, and dynamic variability. Proc Nat Acad Sci USA. 2007;104:16868–73. [PubMed: 17942694]

[9]. Fuller DN, Raymer DM, Rickgauer JP, Robertson RM, Catalano CE, Anderson DL, et al. Measurements of single DNA molecule packaging dynamics in bacteriophage lambda reveal high forces, high motor processivity, and capsid transformations. J Mol Biol. 2007;373:1113–22. [PubMed: 17919653]

[10]. Kindt J, Tzlil S, Ben-Shaul A, Gelbart WM. DNA packaging and ejection forces in bacteriophage. Proc Nat Acad Sci USA. 2001;98:13671–4. [PubMed: 11707588]

[11]. Purohit PK, Inamdar MM, Grayson PD, Squires TM, Kondev J, Phillips R. Forces during bacteriophage DNA packaging and ejection. Biophys J. 2005;88:851–66. [PubMed: 15556983]

[12]. Speir JA, Johnson JE. Nucleic acid packaging in viruses. Curr Opin Cell Biol. 2012;22:65–71.

[13]. Sun S, Kondabagil K, Draper B, Alam TI, Bowman VD, Zhang Z, et al. The Structure of the Phage T4 DNA Packaging Motor Suggests a Mechanism Dependent on Electrostatic Forces. Cell. 2008;135:1251–62. [PubMed: 19109896]

[14]. Liu S, Chistol G, Hetherington CL, Tafoya S, Aathavan K, Schnitzbauer J, et al. A Viral Packaging Motor Varies Its DNA Rotation and Step Size to Preserve Subunit Coordination as the Capsid Fills. Cell. 2014;157:702–13. [PubMed: 24766813]

[15]. Chistol G, Liu S, Hetherington CL, Moffitt JR, Grimes S, Jardine PJ, et al. High degree of coordination and division of labor among subunits in a homomeric ring ATPase. Cell. 2012;151:1017–28. [PubMed: 23178121]

[16]. Moffitt JR, Chemla YR, Aathavan K, Grimes S, Jardine PJ, Anderson DL, et al. Intersubunit coordination in a homomeric ring ATPase. Nature. 2009;457:446–50. [PubMed: 19129763]

[17]. Chemla YR, Aathavan K, Michaelis J, Grimes S, Jardine PJ, Anderson DL, et al. Mechanism of force generation of a viral DNA packaging motor. Cell. 2005;122:683–92. [PubMed: 16143101]

[18]. Black LW. Old, new, and widely true: The bacteriophage T4 DNA packaging mechanism. Virology. 2015;479:650–6. [PubMed: 25728298]

[19]. Zhao H, Christensen TE, Kamau YN, Tang L. Structures of the phage Sf6 large terminase provide new insights into DNA translocation and cleavage. Proc Nat Acad Sci USA. 2013;110:8075–80. [PubMed: 23630261]

[20]. Hilbert BJ, Hayes JA, Stone NP, Xu R-G, Kelch BA. The large terminase DNA packaging motor grips DNA with its ATPase domain for cleavage by the flexible nuclease domain. Nucleic acids research. 2017;45:3591–605. [PubMed: 28082398]

[21]. Hilbert BJ, Hayes JA, Stone NP, Duffy CM, Sankaran B, Kelch BA. Structure and mechanism of the ATPase that powers viral genome packaging. Proc Natl Acad Sci U S A. 2015;112:E3792–9. [PubMed: 26150523]

[22]. Tsay JM, Sippy J, DelToro D, Andrews BT, Draper B, Rao V, et al. Mutations altering a structurally conserved loop-helix-loop region of a viral packaging motor change DNA translocation velocity and processivity. J Biol Chem. 2010;285:24282–9. [PubMed: 20525695]

[23]. Tsay JM, Sippy J, Feiss M, Smith DE. The Q motif of a viral packaging motor governs its force generation and communicates ATP recognition to DNA interaction. Proc Nat Acad Sci USA. 2009;106:14355–60. [PubMed: 19706522]

[24]. Harvey SC. The scrunchworm hypothesis: Transitions between A-DNA and B-DNA provide the driving force for genome packaging in double-stranded DNA bacteriophages. J Struc Biol. 2015;189:1–8.

[25]. delToro D, Ortiz D, Ordyan M, Sippy J, Oh CS, Keller N, et al. Walker-A Motif Acts to Coordinate ATP Hydrolysis with Motor Output in Viral DNA Packaging. J Mol Biol. 2016;428:2709–29. [PubMed: 27139643]

[26]. Berndsen ZT, Keller N, Smith DE. Continuous Allosteric Regulation of a Viral Packaging Motor by a Sensor that Detects the Density and Conformation of Packaged DNA. Biophys J. 2015;108:315–24. [PubMed: 25606680]

[27]. Migliori AD, Keller N, Alam TI, Mahalingam M, Rao VB, Arya G, et al. Evidence for an electrostatic mechanism of force generation by the bacteriophage T4 DNA packaging motor. Nature Communications. 2014;5:4173.

[28]. Duffy C, Feiss M. The large subunit of bacteriophage lambda's terminase plays a role in DNA translocation and packaging termination. J Mol Biol. 2002;316:547–61. [PubMed: 11866517]

[29]. Rao VB, Mitchell MS. The N-terminal ATPase site in the large terminase protein gp17 is critically required for DNA packaging in bacteriophage T4. Journal of Molecular Biology. 2001;314:401–11. [PubMed: 11846554]

[30]. Alam TI, Draper B, Kondabagil K, Rentas FJ, Ghosh-Kumar M, Sun S, et al. The headful packaging nuclease of bacteriophage T4. Molecular microbiology. 2008;69:1180–90. [PubMed: 18627466]

[31]. Mao H, Saha M, Reyes-Aldrete E, Sherman MB, Woodson M, Atz R, et al. Structural and Molecular Basis for Coordination in a Viral DNA Packaging Motor. Cell Rep. 2016;14:2017–29. [PubMed: 26904950]

[32]. Xu R-G, Jenkins HT, Antson AA, Greive SJ. Structure of the large terminase from a hyperthermophilic virus reveals a unique mechanism for oligomerization and ATP hydrolysis. Nucleic acids research. 2017;45:13029–42. [PubMed: 29069443]

[33]. Erzberger JP, Berger JM. Evolutionary relationships and structural mechanisms of AAA+ proteins. Annual Review of Biophysics and Biomolecular Structure. 2006;35:93–114.

[34]. Burroughs AM, Iyer LM, Aravind L. Comparative genomics and evolutionary trajectories of viral ATP dependent DNA-packaging systems. Genome dynamics. 2007;3:48–65. [PubMed: 18753784]

[35]. Lyubimov AY, Strycharska M, Berger JM. The nuts and bolts of ring-translocase structure and mechanism. Curr Opin Struct Biol. 2011;21:240–8. [PubMed: 21282052]

[36]. Hanson PI, Whiteheart SW. AAA+ proteins: have engine, will work. Nature reviews Molecular cell biology. 2005;6:519. [PubMed: 16072036]

[37]. Allemand J-F, Maier B, Smith DE. Molecular motors for DNA translocation in prokaryotes. Current opinion in biotechnology. 2012;23:503–9. [PubMed: 22226958]

[38]. Liu S, Chistol G, Bustamante C. Mechanical operation and intersubunit coordination of ring-shaped molecular motors: insights from single-molecule studies. Biophysical journal. 2014;106:1844–58. [PubMed: 24806916]

[39]. Kjeldgaard M, Nyborg J. Refined structure of elongation factor EF-Tu from Escherichia coli. J Mol Biol. 1992;223:721–42. [PubMed: 1542116]

[40]. Müller CW, Schulz GE. Structure of the complex between adenylate kinase from Escherichia coli and the inhibitor Ap5A refined at 1.9 A resolution. A model for a catalytic transition state. J Mol Biol. 1992;224:159–77. [PubMed: 1548697]

[41]. Cremo CR, Grammer JC, Yount RG. Direct chemical evidence that serine 180 in the glycine-rich loop of myosin binds to ATP. J Biol Chem. 1989;264:6608–11. [PubMed: 2523383]

[42]. Rao VB, Feiss M. The Bacteriophage DNA Packaging Motor. Ann Rev Genetics. 2008;42:647–81. [PubMed: 18687036]

[43]. Walker JE, Saraste M, Runswick MJ, Gay NJ. Distantly related sequences in the alpha- and beta-subunits of ATP synthase, myosin, kinases and other ATP-requiring enzymes and a common nucleotide binding fold. EMBO J. 1982;1:945–51. [PubMed: 6329717]

[44]. Sun S, Kondabagil K, Gentz PM, Rossmann MG, Rao VB. The structure of the ATPase that powers DNA packaging into bacteriophage t4 procapsids. Molecular cell. 2007;25:943–9. [PubMed: 17386269]

[45]. Mitchell MS, Rao VB. Functional analysis of the bacteriophage T4 DNA-packaging ATPase motor. J Biol Chem. 2006;281:518–27. [PubMed: 16258174]

[46]. Mitchell MS, Rao VB. Novel and deviant Walker A ATP-binding motifs in bacteriophage large terminase-DNA packaging proteins. Virology. 2004;321:217–21. [PubMed: 15051382]

[47]. Goetzinger KR, Rao VB. Defining the ATPase center of bacteriophage T4 DNA packaging machine: requirement for a catalytic glutamate residue in the large terminase protein gp17. Journal of molecular biology. 2003;331:139–54. [PubMed: 12875841]

[48]. Story RM, Steitz TA. Structure of the recA protein–ADP complex. Nature. 1992;355:374. [PubMed: 1731253]

[49]. Ortiz D, delToro D, Ordyan M, Pajak J, Sippy J, Catala A, et al. Evidence that a catalytic glutamate and an ‘Arginine Toggle’act in concert to mediate ATP hydrolysis and mechanochemical coupling in a viral DNA packaging motor. Nucleic acids research. 2018;47:1404–15.

[50]. Mitchell MS, Matsuzaki S, Imai S, Rao VB. Sequence analysis of bacteriophage T4 DNA packaging/terminase genes 16 and 17 reveals a common ATPase center in the large subunit of viral terminases. Nucleic Acids Res. 2002;30:4009–21. [PubMed: 12235385]

[51]. Hang JQ, Tack BF, Feiss M. ATPase center of bacteriophage lambda terminase involved in post-cleavage stages of DNA packaging: Identification of ATP-interactive amino acids. J Mol Biol. 2000;302:777–95. [PubMed: 10993723]

[52]. Yang T-C, Ortiz D, Yang Q, De Angelis RW, Sanyal SJ, Catalano CE. Physical and Functional Characterization of a Viral Genome Maturation Complex. Biophysical Journal. 2017;112:1551–60. [PubMed: 28445747]

[53]. Andrews BT, Catalano CE. Strong subunit coordination drives a powerful viral DNA packaging motor. Proc Nat Acad Sci USA. 2013;110:5909–14. [PubMed: 23530228]

[54]. Davidson AR, Gold M. Mutations abolishing the endonuclease activity of bacteriophage λ terminase lie in two distinct regions of the A gene, one of which may encode a “leucine zipper” DNA-binding domain. Virology. 1992;189:21–30. [PubMed: 1534952]

[55]. Yang TC, Ortiz D, Nosaka L, Lander GC, Catalano CE. Thermodynamic Interrogation of the Assembly of a Viral Genome Packaging Motor Complex. Biophys J. 2015;109:1663–75. [PubMed: 26488657]

[56]. Maluf NK, Gaussier H, Bogner E, Feiss M, Catalano CE. Assembly of bacteriophage lambda terminase into a viral DNA maturation and packaging machine. Biochemistry. 2006;45:15259–68. [PubMed: 17176048]

[57]. Keller N, delToro D, Smith DE. Single-Molecule Measurements of Motor-Driven Viral DNA Packaging in Bacteriophages Phi29, Lambda, and T4 with Optical Tweezers In: Lavelle C, editor. Molecular Motors Methods and Protocols. New York, NY: Humana Press; 2018.

[58]. Murialdo H, Davidson A, Chow S, Gold M. The control of λ DNA terminase synthesis. Nucleic acids research. 1987;15:119–40. [PubMed: 3029667]

[59]. Murialdo H Lethal effect of λ DNA terminase in recombination deficient Escherichia coli. Molecular and General Genetics MGG. 1988;213:42–9. [PubMed: 3065611]

[60]. Chow S, Daub E, Murialdo H. The overproduction of DNA terminase of coliphage lambda. Gene. 1987;60:277–89. [PubMed: 2965061]

[61]. von Hippel PH, Berg OG. Facilitated target location in biological systems. J Biol Chem. 1989;264:675–8. [PubMed: 2642903]

[62]. Yang R, Scavetta R, Chang X-b. The hydroxyl group of S685 in Walker A motif and the carboxyl group of D792 in Walker B motif of NBD1 play a crucial role for multidrug resistance protein folding and function. Biochimica et Biophysica Acta (BBA)-Biomembranes. 2008;1778:454–65. [PubMed: 18088596]

[63]. Berndsen ZT, Keller N, Grimes S, Jardine PJ, Smith DE. Nonequilibrium dynamics and ultraslow relaxation of confined DNA during viral packaging. Proc Nat Acad Sci USA. 2014;111:8345–50. [PubMed: 24912187]

[64]. Keller N, Grimes S, Jardine PJ, Smith DE. Single DNA molecule jamming and history-dependent dynamics during motor-driven viral packaging. Nat Phys. 2016;12:757–61. [PubMed: 27540410]

[65]. Keller N, Grimes S, Jardine PJ, Smith DE. Repulsive DNA-DNA interactions accelerate viral DNA packaging in phage phi29. Phys Rev Lett. 2014;112:248101. [PubMed: 24996111]

[66]. Branton D, Deamer DW, Marziali A, Bayley H, Benner SA, Butler T, et al. The potential and challenges of nanopore sequencing. Nanoscience And Technology: A Collection of Reviews from Nature Journals: World Scientific; 2010 p. 261–8.

[67]. Horton RM, Hunt HD, Ho SN, Pullen JK, Pease LR. Engineering hybrid genes without the use of restriction enzymes: gene splicing by overlap extension. Gene. 1989;77:61–8. [PubMed: 2744488]

[68]. Chow S, Daub E, Murialdo H. The overproduction of DNA terminase of coliphage lambda. Gene. 1987;60:277–89. [PubMed: 2965061]

[69]. Sippy J, Patel P, Vahanian N, Sippy R, Feiss M. Genetics of critical contacts and clashes in the DNA packaging specificities of bacteriophages λ and 21. Virology. 2015;476:115–23. [PubMed: 25543962]

[70]. Zissler J, Signer E, Schaefer F. The role of recombination in growth of bacteriophage lambda I. The gamma gene. Cold Spring Harbor Monograph Archive. 1971;2:455–68.

[71]. Yang Q, Catalano CE, Maluf NK. Kinetic Analysis of the Genome Packaging Reaction in Bacteriophage lambda. Biochemistry. 2009;48:10705–15. [PubMed: 19788336]

[72]. Yang Q, Catalano CE. A minimal kinetic model for a viral DNA packaging machine. Biochemistry. 2004;43:289–99. [PubMed: 14717582]

[73]. Rickgauer JP, Fuller DN, Smith DE. DNA as a metrology standard for length and force measurements with optical tweezers. Biophys J. 2006;91:4253–7. [PubMed: 16963512]

[74]. delToro D, Smith DE. Accurate measurement of force and displacement with optical tweezers using DNA molecules as metrology standards. Appl Phys Lett. 2014;104:143701. [PubMed: 25316922]

[75]. Fuller DN, Gemmen GJ, Rickgauer JP, Dupont A, Millin R, Recouvreux P, et al. A general method for manipulating DNA sequences from any organism with optical tweezers. Nucleic Acids Res. 2006;34:e15. [PubMed: 16452295]

[76]. Baker NA, Sept D, Joseph S, Holst MJ, McCammon JA. Electrostatics of nanosystems: application to microtubules and the ribosome. Proceedings of the National Academy of Sciences. 2001;98:10037–41.

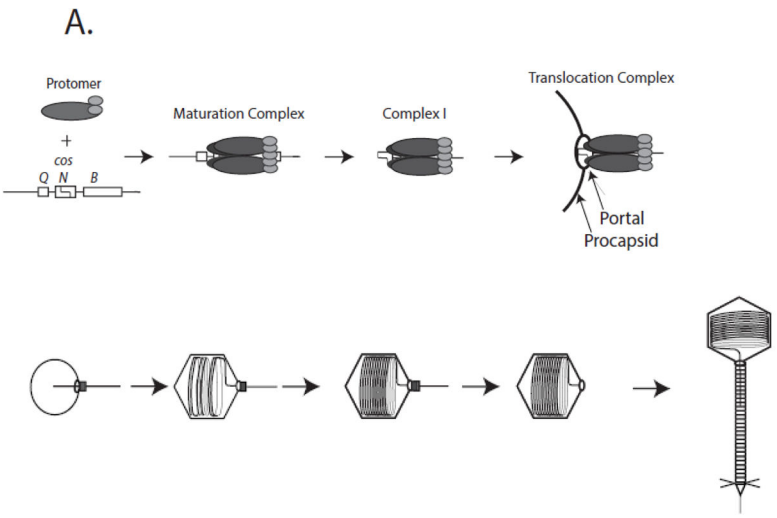

B.

Virus (Phage)	Classical Walker A Motif	Classical Walker B-Catalytic Glutamate Motif	Accession or PDB Number
	(G/A)XXXXGK(T/S)	ΦΦΦΦD-E	
Lambda	^{76}-KSARVGYS-^{83}	^{174}-VAGYD-E-^{179}	P03708.1
T4	^{160}-LSRQLGKT-^{167}	^{251}-MIYID-E-^{256}	P17312.1
Sf6	^{22}-GGRGSGKS-^{29}	^{114}-ICWVE*-E-^{119}	PDB: 4IEE_A
P74-26	^{37}-LGRQSGKS-^{44}	^{145}-FVILD-E-^{150}	PDB: 4ZNI, 4ZNJ, 4ZNK, 4ZNL
D6E*	^{41}-GSIRAGKT-^{48}	^{138}-GMFFD-E-^{143}	PDB: 5OE8, 5OE9, 5OEA, 5OEB, 5OEE
Phi29	^{24}-GARGIGKS-^{31}	^{114}-TIVFD-E-^{119}	PDB: 5HD9

Figure 1. Model of lambda genome packaging.

A-Upper: Packaging initiation. The terminase protomer is a tight association of two TerS$^{\lambda}$ subunits and one TerL$^{\lambda}$ subunits. In the N-terminal domain (NTD) of TerS$^{\lambda}$ is a winged helix-turn-helix DNA binding motif and the TerS$^{\lambda}$ dimerization interface. The TerS$^{\lambda}$ C-terminal domain (CTD) includes a functional domain for interacting with TerL$^{\lambda}$'s N-terminus. TerL$^{\lambda}$ consists of two globular domains connected by a linker. The TerL$^{\lambda}$ NTD contains the DNA packaging ATPase and the CTD contains the maturation endonuclease. Four protomers form into a ring-like structure at the *cos* site of a lambda genome concatemer, assembling the maturation complex. Maturation complex assembly involves interactions of TerS$^{\lambda}$ with *cosB*, and the TerL$^{\lambda}$ endonuclease with *cosN*, and requires ATP and/or IHF. Following duplex nicking by TerL$^{\lambda}$ and ejection of the upstream, *cosQ*-containing DNA end yields the post-cleavage complex (Complex I). Complex I docks at the portal of an empty procapsid, producing the packaging motor complex. Complex I docking involves an interaction between the TerL$^{\lambda}$ C-terminal tether and the portal protein. Docking activates the packaging ATPase, which powers translocation of DNA into the procapsid shell. We note that the stoichiometry of the protomer subunits bound to the procapsid, along with the subunit arrangement in the maturation complex, remain speculative at this time. A-Lower: Translocation and virion assembly. Progression of translocation is shown proceeding left to right. When ~30% of the DNA has been translocated, procapsid expansion is

triggered, and translocation proceeds until the next *cos* along the concatemer is encountered. Interactions between the translocating terminase and *cosQ* and *cosN* lead to nicking of the downstream *cos*, and terminase undocking. Addition of gpW and gpFII to the portal is followed by tail attachment, generating a mature virion. B. ATPase motif sequences. Walker B motif and catalytic glutamate ASCE sequences are given for TerLs discussed in this paper. Beginning and ending residue numbers are given in superscripts. *Note that $TerL^{Sf6}$ contains a deviant glutamate (red) rather than the canonical aspartate found in most ASCE Walker B sequences

	L			
A-V		S		E*
V174	A175	G176	Y177	D178
G-V		C-W		A
G-I		E-K		F
A-P		L-C		K
A-Q		V-F		L
C-M		G-G		N
C-Y		L-E		P
D-S		R-G		S
E-D		R-R		T
G-E		V-G		W
G-G			V	
P-A				
R-D				
R-R				
S-D				
S-F				
T-E				
L-L				
Y-R				
P				

Phage Yield (pfu/cell) (Relative to WT)	Color Key
1 ~ 10^{-1}	Viable
10^{-1} ~ 10^{-2}	Lethal
10^{-2} ~ 10^{-3}	Lethal
10^{-3} ~ 10^{-5}	Lethal
10^{-5} ~ 10^{-7}	Lethal
< 10^{-7}	Lethal

Figure 2: Effects of residue changes in the Walker B motif on virus yield.

Left table lists the mutants tested and a color-key is used to indicate the range of detected degrees of impairment expressed in terms of phage yield in plaque forming units per cell relative to WT (where the WT activity is defined to be 1). Right table lists the color-key that indicates the relative phage yields. Dark gray color is used to designate cases where no phage yield was detected (i.e., below the level of sensitivity of the assay). Pairs of codons were mutagenized for codons 174-175, and for 176-177, though single codon changes were made for the V174P, A175L, G176S, and Y177V mutants. Wildtype terminase sponsored yields of 3 – 10 λ *A*am/induced cell. Two of the mutants, V174V+A175L and V174P +A175A were effectively single mutants because each contained a same-sense codon change in addition to a mutation causing a residue change. The same-sense changes were to codons with usage frequencies similar to that of the wildtype codon. For example, the codon changes producing TerL$^{\lambda}$-V174V+A175L were GUG+GCG→GUA+CUG. The codon usages in *E. coli* for the wildtype and same-sense valine codons are 2.4% and 1.2%, respectively. The GUA codon is occurs twice in the wildtype *A* gene, indicating that the change to this codon is unlikely to affect gene expression. Accordingly, these two mutants are listed as single mutants V174P and A175L.

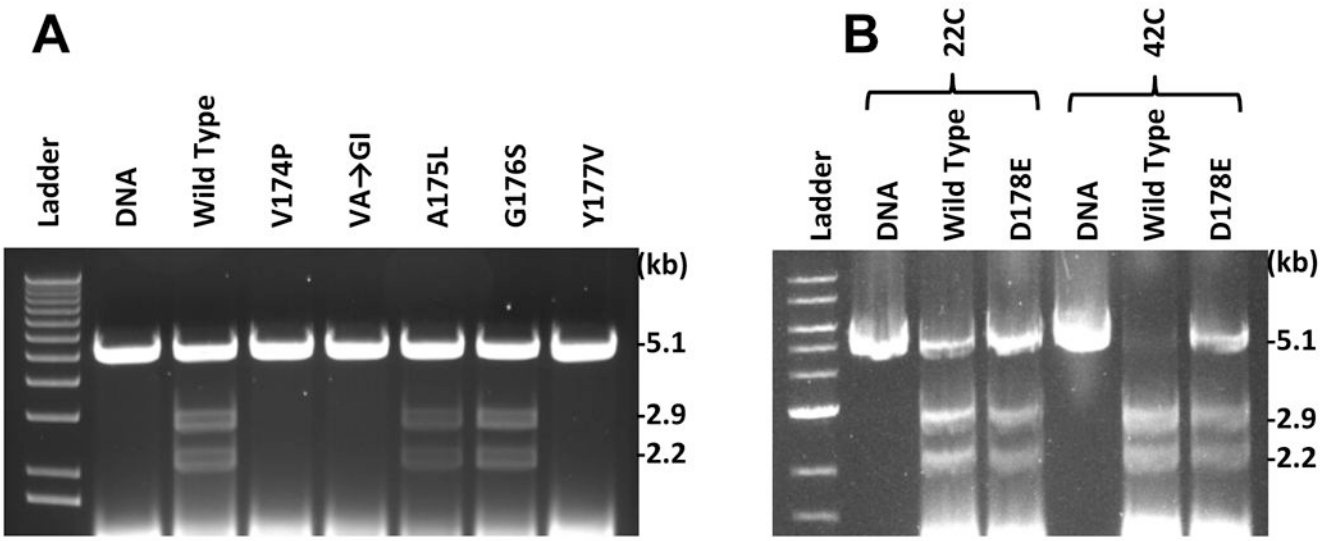

Figure 3. ***In vitro cos*** **cleavage activity of terminases.**

Cleavage assay results for selected mutants. Cleavage of the 5.1 kb substrate DNA at *cos* produces 2.9 and 2.2 kb product DNAs. A. Standard reactions done at 30°C. B. Reactions done at 22°C and 42°C with the cold-sensitive gpA D178E terminase. Unlabeled lanes are 1 kb ladder (New England Biolabs). The A175L extracts contained an EDTA-free protease inhibitor cocktail (“cOmplete Mini”, Roche, Inc.) at the recommended concentration.

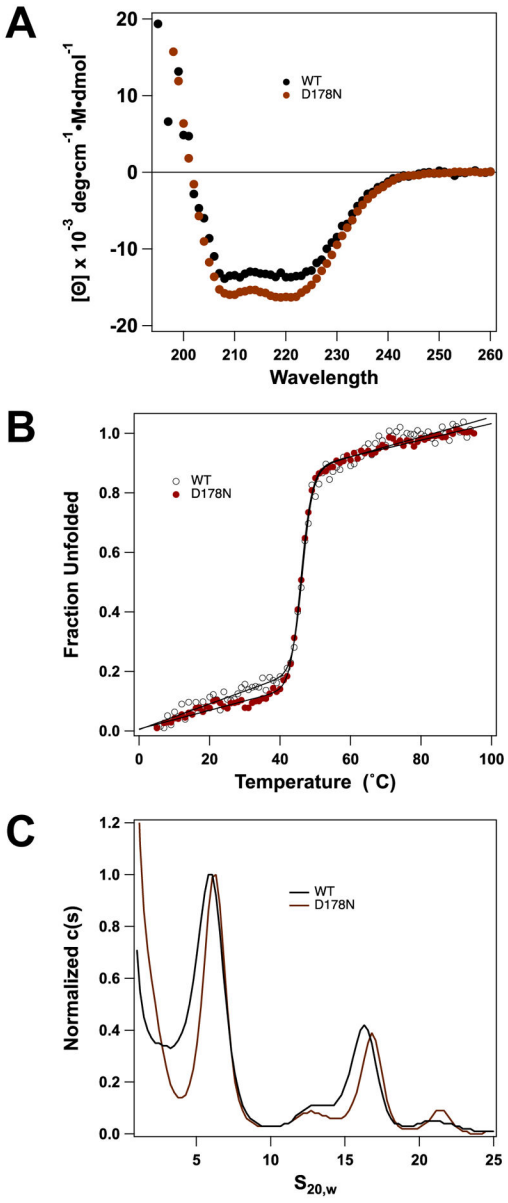

Figure 4. Assessment of protomer folding and thermal stability.

(A) CD spectra show that secondary structure compositions for TerL$^{\lambda}$D178N are similar to WT (~37% α-helical, ~17% β-sheet). **(B)** Thermal denaturation was monitored by CD (222 nm) and the data were analyzed as described in Materials and Methods (solid lines). The data show that the TerL$^{\lambda}$-D178N mutant has thermal stability similar to WT; T_m= 46.4 ± 0.21°C and T_m= 46.0 ± 0.1°C, respectively. (**C**) SV-AUC analysis indicates the TerL-D178N Walker B mutant has no major assembly defect. The WT protomer (~6S) is in slow equilibrium with a tetramer of protomers.

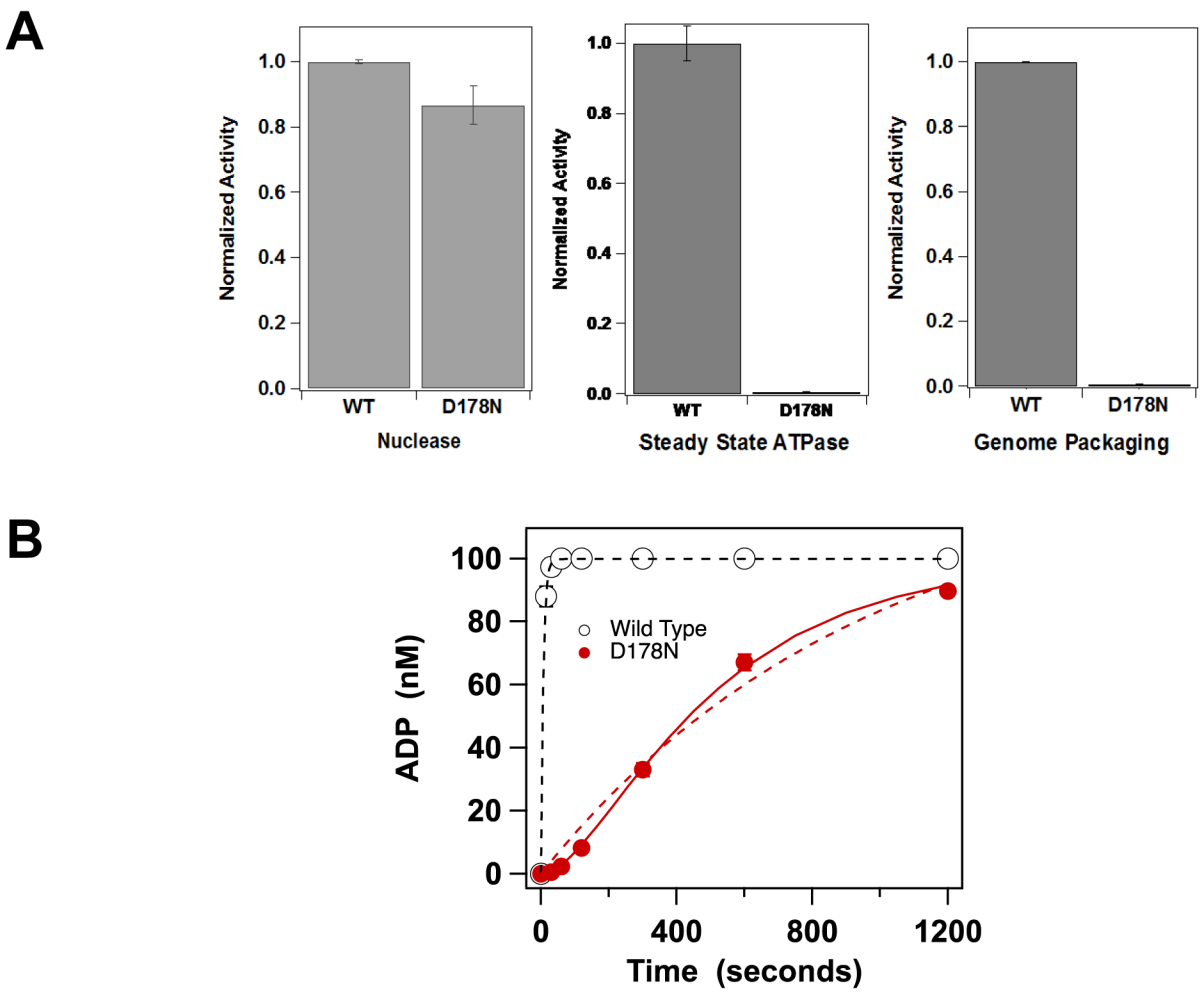

Figure 5. Catalytic Activity of TerL$^{\lambda}$-D178N terminase.

cos-cleavage nuclease, DNA packaging and steady-state ATPase activities were performed as described in Materials and Methods. Each bar represents the average of three separate experiments with error-bars indicating the standard errors in the mean. **(B)** Single turnover ATP hydrolysis was performed as described in Materials and Methods; the reaction was initiated by the addition of enzyme. The reaction time courses for WT (○) is well described by a single-turnover, monophasic exponential model (solid line). In contrast, TerL$^{\lambda}$-D178N displays a significant lag phase (●), which is poorly described by the simple model (see text; dashed red line). The mutant data are better described by the three-state model that includes a slow step prior to catalysis (Equation 1, solid red line). The kinetic constants derived from non-linear regression analysis of each data set is presented in Table 3.

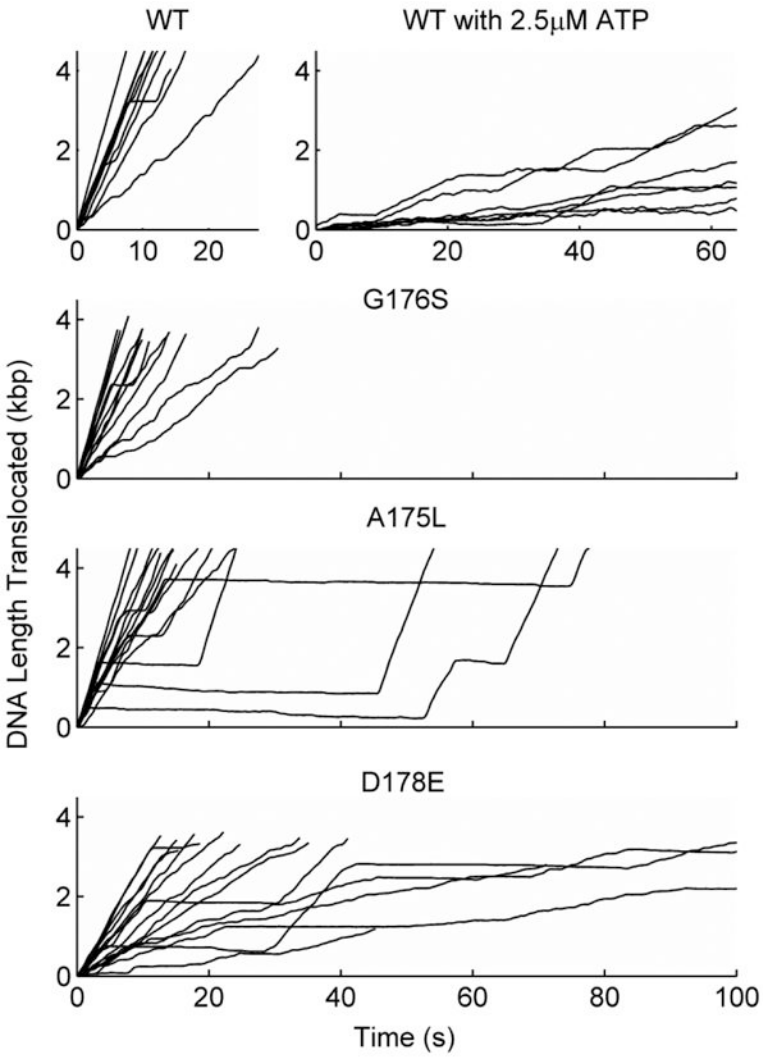

Figure 6. Examples of single DNA molecule translocation measurements for wildtype terminase (WT) and mutants G176S, A175L, and D178E as indicated.

All plots are of DNA length translocated (kpb) vs. time (seconds) and the bottom three plots share the same horizontal axis tick labels as indicated on the bottom plot. All measurements are with saturating ATP (500 μM) except for the WT measurements labeled 2.5 μM ATP.

Terminase	# of Events	Motor Velocity (bp/s)	Packaging Rate (bp/s)	Pause Frequency (pauses/kbp)	Pause Duration (s)	Slip Frequency (slips/kbp)	Phage Yield
WT	53	400 ± 20	350 ± 20	1.2 ± 0.4	2 ± 0.1	0.5 ± 0.1	1
G176S	36	420 ± 20	390 ± 60	0.7 ± 0.3	2.3 ± 0.5	0.11 ± 0.05	2
A175L	30	360 ± 20	270 ± 50	1.6 ± 0.7	4.7 ± 0.4	1.1 ± 0.5	0.6
D178E	72	159 ± 8	120 ± 10	3.6 ± 0.7	3.8 ± 0.4	0.7 ± 0.2	0.4
WT - 5μM ATP	9	130 ± 20	50 ± 20	8 ± 2	1.58 ± 0.09	5 ± 1	n/a
WT - 2.5μM ATP	13	79 ± 6	24 ± 7	13 ± 2	1.8 ± 0.1	7 ± 1	n/a
^{174}VA^{175}→GI	0	0	0	0	0	0	3.3×10^{-5}
V174P	0	0	0	0	0	0	$< 10^{-7}$
Y177V	0	0	0	0	0	0	$< 10^{-7}$
D178A	0	0	0	0	0	0	$< 10^{-7}$
D178N	0	0	0	0	0	0	$< 10^{-7}$

Figure 7. Effects of limiting ATP and Walker B residue changes on motor velocity and pausing.

Pausing frequency vs. motor velocity for wildtype terminase (WT) and mutants (indicated by labels on top of plot). Results for mutant V80A from a previous study are shown for comparison. Measurements were done with saturating ATP (500 μM) and, for WT, also with sub-saturating ATP (5 μM and 2.5 μM, where indicated). Dashed lines indicate pausing frequencies for WT with the different ATP concentrations. Note that the V80A mutant (measured with 500 μM) follows the trend that exhibited by the WT of increasing pause frequency with decreasing motor velocity, but mutant D178E does not.

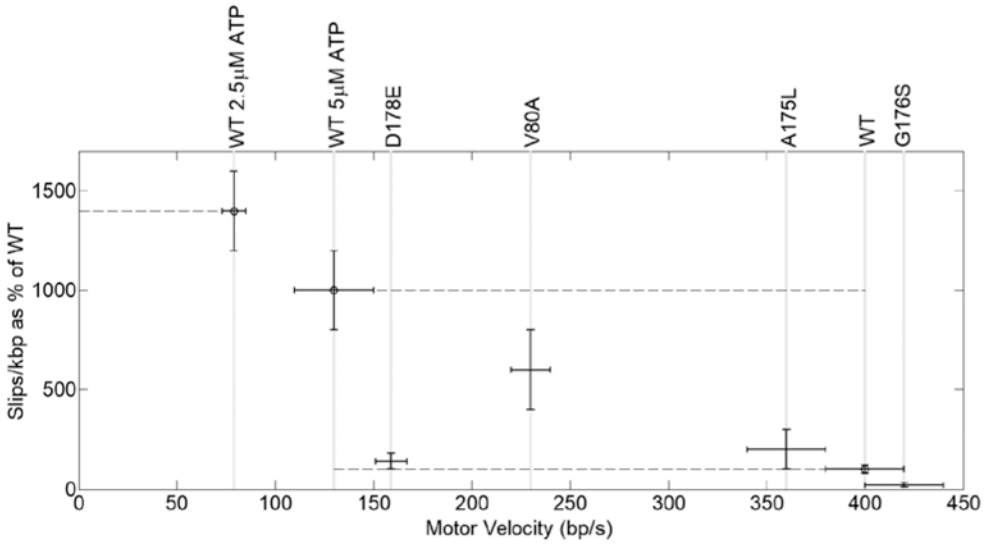

Figure 8. Metrics of DNA translocation activity for wildtype (WT) and mutant terminases determined by analysis of the optical tweezers measurements.

The results are reported as mean values, except for the last column that reports viral assembly activity (phage yield per cell) as a fraction of WT (the color codes in this column are the same as used in Figure 2). All measurements were done with saturating ATP (500 μM), except for those labeled WT 5 μM ATP and WT 2.5 μM ATP, which report WT measurements with lowered [ATP]. Uncertainties are expressed as standard error in the mean.

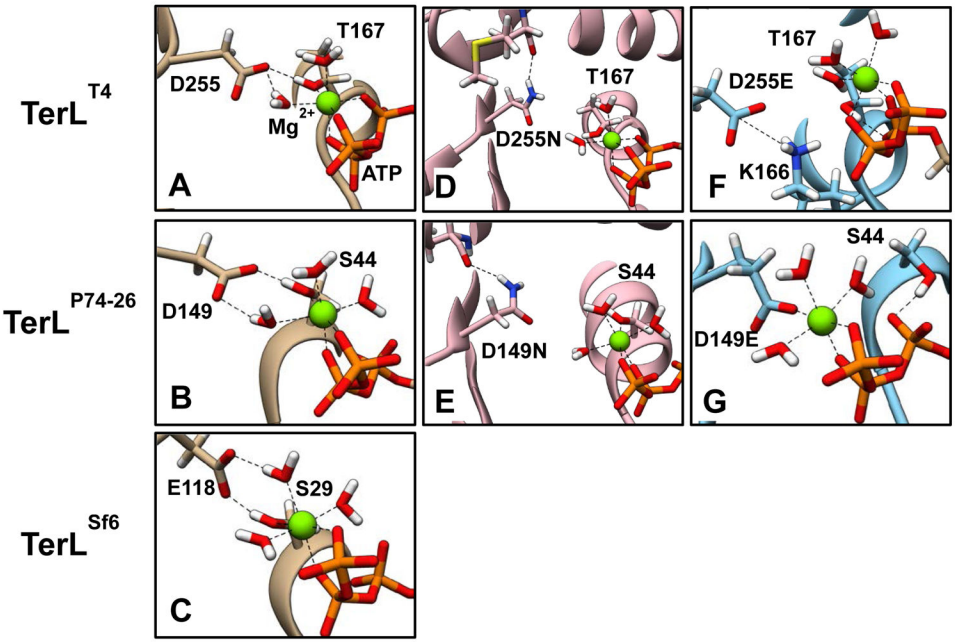

Figure 9. Molecular dynamics simulations identify importance of interaction between WA and WB motifs.

MD simulations of the WT T4 (A), P74-26 (B), and Sf6 (C) terminase proteins highlight a conserved interaction between the WB Asp/Glu carboxylate group and the WA Thr/Ser hydroxyl group. This interaction helps the binding pocket close around the bound Mg^{2+}-ATP as part of the tight binding transition. This interaction is maintained even with the deviant WB Glu found in Sf6 terminase due to a larger backbone-to-backbone distance (see Table 2). Simulations of Asp→Asn variants of the T4 (D) and P74-26 (E) terminase proteins show that these groups remain isolated to the WB motif and do not interact with the WA motif as found in WT. Simulations of the Asp→Glu variants of the T4 (F) and P74-26 (G) terminase proteins suggest unique defects arise in the binding pocket. The simulated T4 mutant D255E interacts with the critical WA K166, similar to mutant crystal structure (see Figure S4). The simulated P74-26 mutant D149E chelates Mg^{2+} directly as opposed to via a bound water molecule, displacing S44 (compare with panel B).

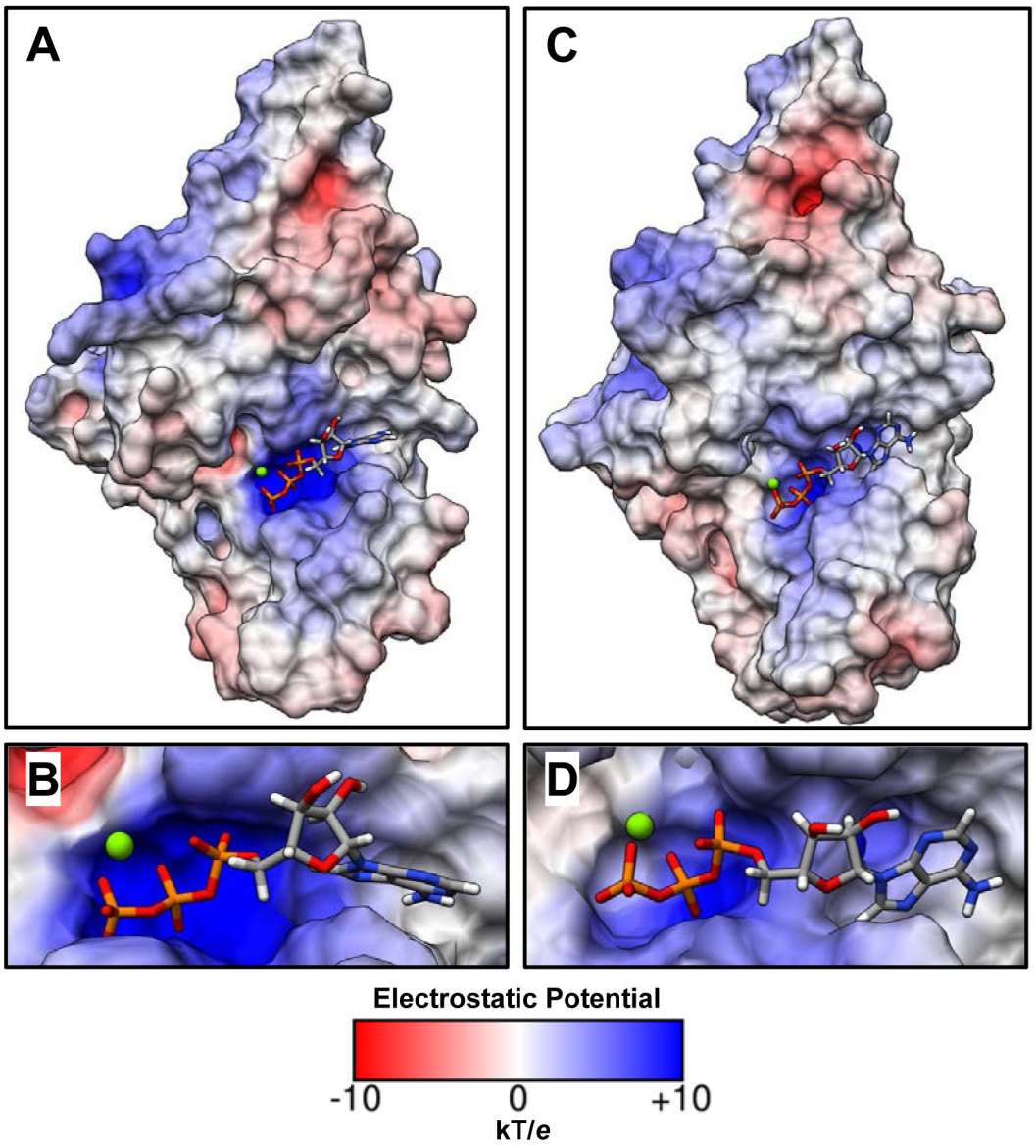

Figure 10. Electrostatic potential of WT and mutant P74-26 TerL binding pockets.

(A) The solvent-excluded surface of the WT P74-26 TerL ATPase domain colored according to its electrostatic potential. (B) A close up of the WT ATP binding pocket. (C) The solvent-excluded surface of the WB Asp→Glu variant P74-26 TerL ATPase domain colored according to its electrostatic potential. (D) A close up of the Asp→Glu variant ATP binding pocket. When compared to the WT binding pocket (B), the Asp→Glu binding pocket (D) has reduced positive electrostatic potential around the γ-phosphate of ATP due to the rearrangements described in Figure 9G. This could reduce the polarization of the γ-phosphate and destabilize the transition state, explaining the observed impairment of ATP hydrolysis observed experimentally in lambda phage.

Table 1.

Single Turnover ATPase Kinetic Analysis.

The data presented in Figure 5B were fit to a monophasic reaction time course and a three-state kinetic model as described in Materials and Methods. The derived rate constants are presented with standard deviations as indicated.

Enzyme	*Monophasic Model*	*Three-State Model*	
	k_{obs} (s^{-1})	k_1 ($M^{-1}s^{-1}$)	k_2 (s^{-1})
WT	(0.139 ± 0.016)	-	-
D178N	(1.0 ± 0.4) x 10^{-3}	(1.7 ± 0.2) x 10^4	(2.4 ± 0.1) x 10^{-3}
R79A	-	(1.3 ± 0.9) x 10^4	(5.3 ± 2.9) x 10^{-3}

Table 2.

Backbone distance (Cα-Cα) of the C-terminal WB D/E to the C-terminal WA T/S.

All values are reported in Å. Values from MD simulations are averaged across three independent 100 ns simulations, and the uncertainty is the standard error in the mean.

Terminase	Apo Crystal	Apo MD	ATP-Bound Crystal	ATP-Bound MD
P74-26	8.08	8.64 ± 0.10	6.54	6.54 ± 0.03
T4	9.35*	9.45 ± 0.07	9.55*	7.11 ± 0.01
Sf6	7.91	7.63 ± 0.06	7.90	7.91 ± 0.07
P74-26 D149E	-	-	-	7.21 ± 0.10
T4 D255E	-	-	-	9.22 ± 0.20

*$TerL^{T4}$ crystal structures are of the WB D255E/E256D double mutant; D255E is directly involved in this measurement.